



Thermodynamics, optical properties, and coordination of lanthanoids with hydroxyquinolate functionalised receptor

Neha Kumari¹ · Minati Baral¹ · Dinesh Kumar¹ · B. K. Kanungo²

Received: 27 January 2024 / Accepted: 27 February 2024 / Published online: 10 April 2024
© The Author(s), under exclusive licence to Springer Nature B.V. 2024

Abstract

Two new lanthanide complexes with the general formula $[\text{Ln}(\text{hqtsc})_2\text{Cl}]$, where $\text{Ln} = \text{Eu}^{3+}/\text{Tb}^{3+}$ and hqtsc is (E)-2-((8-hydroxyquinolin-2-yl)methylene)hydrazine-1-carbothioamide have been synthesized. The structures of the complexes have been elucidated through IR, ^1H NMR, ^{13}C NMR and HR-mass spectroscopy. The coordination behavior of the ligand was investigated with proton and two trivalent lanthanides, Eu(III) and Tb(III), by potentiometric and spectrophotometric methods in a highly aqueous medium. The studies reveal that the two lanthanides form complexes of the type ML_2H_2 , ML_2H_1 , ML_2 , ML_2H_{-1} , and ML_2H_{-2} . The high formation constants of ML with $\log \beta = 26.55$ and 27.13 indicate that these complexes will become promising candidates for chelation therapy, radioimmunotherapy, and other biomedical applications. Further, the change in colour and electronic spectra of the complexes in the presence of anions showed the selective colorimetric sensing ability towards H_2PO_4^- (orange/yellow \rightarrow colorless) and CN^- (orange/yellow \rightarrow red). The DFT studies were also carried out to establish the structure, bonding, and sensing mechanism of the complexes.

Keywords Europium · Terbium · Formation constants · Colorimetric anion sensor · DFT · TDDFT

Introduction

The chemistry of trivalent lanthanides is gaining attention due to their unique luminescent and magnetic characteristics [1–4]. Lanthanoid complexes exhibit luminescence in the near-UV region (Ce^{3+} and Gd^{3+}), near-infrared (Nd^{3+} , Er^{3+} , and Yb^{3+}) range, and also exhibit high luminescence in the visible range (Eu^{3+} and Tb^{3+}). Undesirably, the trivalent lanthanides show low luminescence intensity with a low molar absorptivity (ϵ) ($< 10 \text{ L mol}^{-1} \text{ cm}^{-1}$) because of the Laporte forbidden f-f transitions [5, 6]. However, by coordinating lanthanide ions to a chromophoric unit that acts as an antenna and consequently transfers its energy effectively to the metal ion can avoid these limitations [7, 8]. Based on such antenna effect, the lanthanide complexes demonstrating sharp and strong luminescence have been developed with many organic ligands such as β -diketone [9] carboxylate,

[10] calixarenes, cryptands including 8-hydroxyquinolate (8HQ) [11]. Moreover, these lanthanide frameworks with organic chromophores have aroused the interest of researchers for their interaction with foreign molecules like anions and the associated color changes. Lanthanide complexes are oxophilic and carry a positive charge, interacting with anions through strong electrostatic forces [12]. The 8-hydroxyquinoline and its derivatives are studied extensively due to their crucial role in various biological actions that include antibacterial, antioxidizing, anticancer, and antifungal properties [13–15], and most importantly, cancer diagnosis and therapy [16, 17]. 8HQ-based Ln(III) chelates are also effective for precise detection and selective sensing of anions of biological importance [18]. The design and development of chemosensors for selective detection of anions have received attention in supramolecular chemistry because of their critical importance in a wide range of environmental, biological, and chemical processes [19–21]. The binding of sensors with the anions leads to changes in one or more features of the system, such as colorimetric changes [22–24], fluorimetric changes [25–27], or changes in electrochemical properties [28–30]. These anion probes are capable of recognizing anions with different sensitivities, and the probe–anion interactions can be easily visualized via naked-eye colorimetric

✉ Minati Baral
minatibnitkkr@gmail.com

¹ National Institute of Technology, Kurukshetra,
Haryana 136119, India

² Sant Longowal Institute of Engineering and Technology,
Longowal, Sangrur, Punjab 148106, India

or luminescent responses [31]. Among various ions, phosphates in their inorganic (H_2PO_4^- , HPO_4^{2-} , PO_4^{3-} and PPi) and organic (ATP, ADP, and AMP) forms are essential in biology due to their defined role in signal transduction, storage of energy, and gene development processes [32–34]. However, excessive levels of phosphate in the human body lead to several disorders, such as hyperphosphatemia, soft tissue calcification, cardiovascular problems, renal failure, and hence higher rates of mortality and morbidity [35–39]. Cyanide is another toxic anion that is lethal for living beings. The global output of cyanide is quite large because of its wide industrial applications in manufacturing paper, plastics, textiles, dyes, electroplated metals, and, most importantly, the metallurgy of gold and silver. While cyanide poisoning is uncommon, it can occur as a result of inhaling smoke from industrial fires or using industrial wastes-polluted water, as well as working in the mining sectors [40–42]. Cyanide's extreme toxicity stems from its ability to impede oxygen intake by iron-containing enzymes such as cytochrome oxidase and hemoglobin by interacting with the iron present in them and thereby obstructing oxygen delivery and cellular respiration, resulting in death due to cerebral hypoxia [43, 44]. Some lanthanide-based luminous sensors have been reported for their selective detection of anions such as bicarbonate, chloride, and nitrates [45–49], and a few trivalent Eu and Tb probes for detecting phosphate ions [50–53]. However, to our knowledge, no documentation on lanthanide chemosensors for the simultaneous detection of phosphate and cyanide ions via naked-eye responses has been reported.

In the above view, two new trivalent lanthanide complexes (Eu and Tb) comprising a hydroxyquinoline-based ligand (E)-2-((8-hydroxyquinolin-2-yl)methylene)hydrazine-1-carbothioamide (hqtsc) have been developed and characterized that can simultaneously detect dihydrogen-phosphate (H_2PO_4^-) and cyanide (CN^-) ions colorimetrically. In-depth studies on the structure, bonding, solution thermodynamics, and electronic properties of the metal chelates have been done through experimental and DFT approaches. Further, the sensing mechanism of the probes towards H_2PO_4^- and CN^- , which go along with the spectral and DFT evidence, have been proposed.

Result and discussion

Synthesis

The synthesis routes for preparation of the ligand hqtsc (**1**) and complexes $\text{Eu}(\text{hqtsc})_2\text{Cl}$ (**2**) and $\text{Tb}(\text{hqtsc})_2\text{Cl}$ (**3**) are shown in Scheme 1.

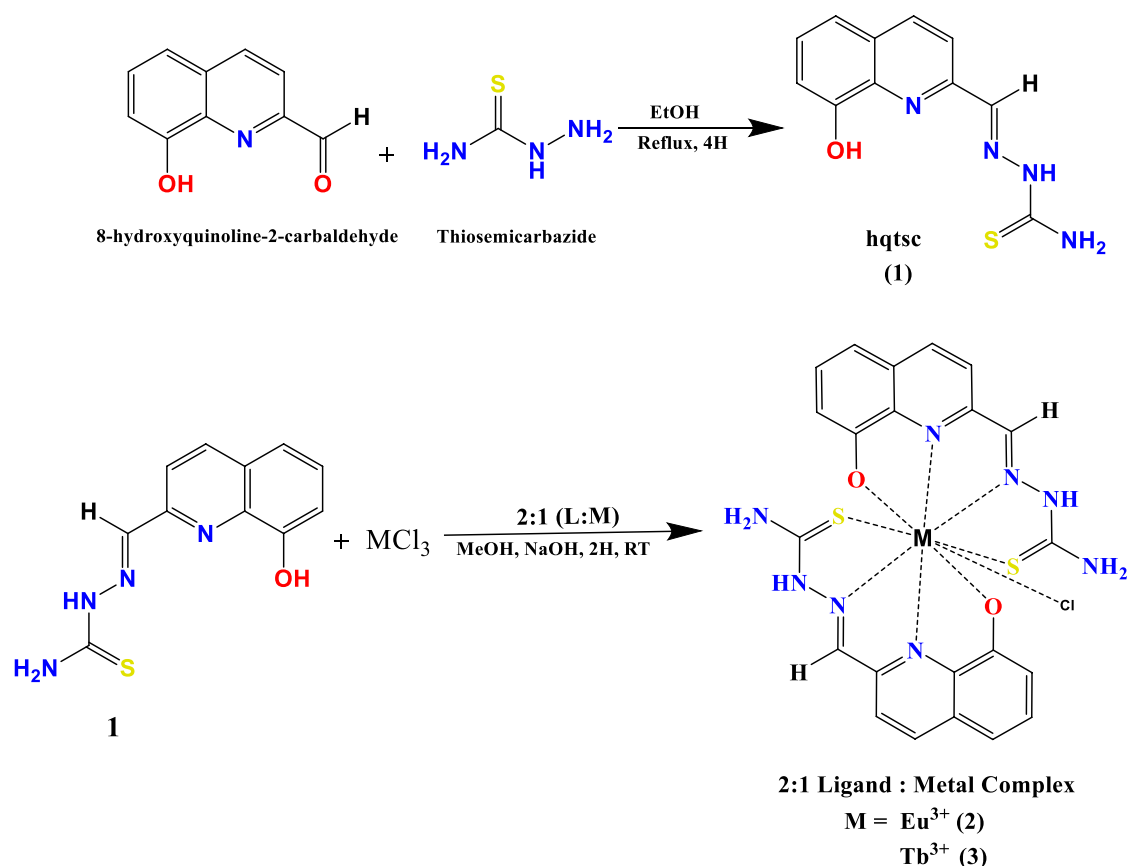
The ligand hqtsc was synthesized by condensation of 8-hydroxyquinoline-2-carbaldehyde with thiosemicarbazide in an ethanol medium by following the literature

[54]. The complexes, $\text{Eu}(\text{hqtsc})_2\text{Cl}$ (**2**) and $\text{Tb}(\text{hqtsc})_2\text{Cl}$ (**3**), were synthesized by reacting the chloride salts with the ligand hqtsc in methanol. The complexes are stable at room temperature, soluble in DMSO and DMF solvents, and characterized by advanced techniques like IR, ^1H NMR, ^{13}C NMR, and mass spectroscopy, confirming the molecular formulations. The characterization details of **1**, **2**, and **3** are provided in supplementary information (Figs. S1–S10).

Characterization

IR spectra

The FT-IR spectrum of the ligand (hqtsc) and its lanthanide complexes have well-defined vibrational frequencies in the IR region. The characteristic peak of azomethine group $\nu(\text{N}=\text{CH}-)$ at 1539 cm^{-1} confirms the successful condensation of 8-hydroxyquinoline-2-carbaldehyde with thiosemicarbazide. Also, the appearance of peaks at 3248 cm^{-1} and 3387 cm^{-1} due to the symmetric and asymmetric stretch of the terminal $-\text{NH}_2$ group, along with a broad band at 3600 cm^{-1} due to the presence of hydroxide group ($-\text{OH}$) supports the formation of ligand hqtsc. The thiosemicarbazone hqtsc, in principle, can exhibit thiol-thione tautomerism; the peak at 1327 cm^{-1} is due to $\nu(\text{C}=\text{S})$ along with secondary N-H stretch present at 3153 cm^{-1} corresponds to the presence of thione form. Further, a weak -SH stretching frequency at 2800 cm^{-1} and C-S stretching band at $\sim 939\text{ cm}^{-1}$ corresponding to thiol tautomer suggest that the ligand exists in both forms at room temperature. On complexing with the lanthanides, the stretching vibration of the imine linkage underwent a slight shifting from 1539 cm^{-1} to 1535 cm^{-1} in both complexes, indicating the imine-N's participation in complex formation. The band at $\sim 3600\text{ cm}^{-1}$ disappeared due to deprotonation of -OH group upon complexation with the metal ions. Further, the shifting of $\nu\text{C}=\text{S}$ from 1327 cm^{-1} (ligand) to 1273 and 1271 cm^{-1} , along with the shifting of $\nu\text{N}-\text{H}$ from 1353 cm^{-1} to 3161 cm^{-1} and 3163 cm^{-1} in complexes **2** and **3**, respectively were noticed clearly. However, no peak due to $\nu\text{C}-\text{S}$ of the ligand was observed in Eu^{3+} and Tb^{3+} complexes, indicating the existence of the thione tautomer form. The sharp peaks due to $\nu\text{M}-\text{O}$ vibrations observed at 439 cm^{-1} and 441 cm^{-1} , and $\nu\text{M}-\text{N}$ vibrations at 495 and 497 cm^{-1} correspond to **2** and **3**, respectively. Due to the instrument limitations, the stretching vibrations $\nu\text{M}-\text{S}$ and $\nu\text{M}-\text{Cl}$ appearing in the region of $100-300\text{ cm}^{-1}$ could not be produced. The IR spectra of the Tb-complex showed a broad band between 3500 and 3200 cm^{-1} , suggesting the presence of lattice water in complex **3**, which was missing in complex **2**. The thermogravimetric analysis (TGA) also proved the existence of lattice water in the Tb-complex.



Scheme 1 Synthetic scheme of hqtsc (1) and its complexes with Eu³⁺ (2) and Tb³⁺ (3)

¹H and ¹³C NMR Spectra

The ¹H and ¹³C NMR spectra of the ligand hqtsc and complexes were recorded in the deuterated DMSO-D₆ medium. Nine protons and eleven carbon atoms with chemically different environments were observed; the chemical shift corresponding to each signal has been given in the experimental section. Due to the paramagnetism of Eu³⁺ and Tb³⁺ ions, the broadening in the signals, along with a considerable downfield shift, was observed in the spectra. The broadening in the protons signals near paramagnetic lanthanides depends on (a) dipolar interactions and (b) Curie-spin relaxation; the line width is also governed by the strength of the magnetic field and the inverse sixth power of corresponding proton-lanthanide distance [55]. In the case of the Eu(III) complex, the electron relaxation time was less, so the complex was expected to give sharp signals as compared to Tb(III) complex, where the relaxation time is high due to spin-spin splitting therefore, more signal broadening is expected [55]. The ¹H NMR spectrum of complex 2 shows sharp signals (Fig. S6), where the -OH proton peak is absent, confirming the ligand-metal coordination. Further, the peak for the secondary -NH- proton of thiosemicarbazide is seen with

more downfield shifting (at 11.02 ppm), which means the ligand coordinates with lanthanides through the 'S' atom and not with secondary -NH- group. The NMR spectrum of complex 3 was broad and did not show high-resolution signals (Fig. S7).

Mass Spectra

High-resolution mass spectrum (HR-MS) recorded for the ligand hqtsc showed an exact mass peak at 247.0664, which matches with the L+H calculated value 247.0655, corresponding to the exact mass of the ligand. The spectrum of Eu(hqtsc)₂Cl showed a peak at 643.0215, complementary to [Eu(hqtsc)₂]⁺ (calculated mass = 643.0190) after fragmentation of Cl atom. Further, the peak corresponding to Eu(hqtsc)+1 appeared at 398.9447 after the dissociation of one of the ligands. In the mass spectrum of Tb(hqtsc)₂Cl, the signal at 649.0266 can be assigned to [Tb(hqtsc)₂]⁺ formulation and the peak at 404.952 corresponds to Tb(hqtsc)+1 for. The molecular ion peaks in the mass spectra agreed with their calculated mass. The presence of one Cl atom in each complex was confirmed by quantitative estimation of Cl⁻ as AgCl by use of AgNO₃ reagent [56].

Thermogravimetric Analysis

Thermogravimetric (TG) analysis is one of the most effective techniques to check the presence of water molecules, and it can also differentiate the non-coordinated water molecules (80–150 °C) from the coordinated ones (150–220 °C) [57]. The TGA was performed under a nitrogen atmosphere from temperature 40 °C to 500 °C with a heating rate of 20 °C per minute. Eu^{3+} complex was found thermally stable up to 230 °C, indicating the absence of any lattice or coordinated water, including solvent molecules. Degradation of **2** was seen from 230 to 327 °C with 18.10% equivalent weight loss. The second weight loss starts from 330 °C to 500 °C and above (Fig. S11). On the other hand, TG curves of the Tb(III) complex (Fig. S12) reveal an initial mass loss of 1.42% occurred in the range of 110–160 °C, corresponding to 0.5 mol of water molecules present in the lattice. The second loss happened from 220 to 470 °C, corroborating a 20.66% weight loss (Fig. S12).

Electronic absorption spectra

The UV-visible spectra of hqtsc and its complexes, recorded in 10^{-5} M DMF solution, are shown in Fig. 1. The ligand showed a band at 346 nm ($\epsilon = 32951 \text{ M}^{-1} \text{ cm}^{-1}$) with a shoulder at 314 nm ($\epsilon = 25407 \text{ M}^{-1} \text{ cm}^{-1}$), assigned as $\pi \rightarrow \pi^*$ transitions. Upon coordination with lanthanides, the bands at 314 and 346 nm showed an increase in the molar absorbance along with two new absorption bands in the visible range at 418 nm ($\epsilon = 12,372 \text{ M}^{-1} \text{ cm}^{-1}$ for **2** and $16,907 \text{ M}^{-1} \text{ cm}^{-1}$ for **3**) and 490 nm ($\epsilon = 4184 \text{ M}^{-1} \text{ cm}^{-1}$ for **2** and $6054 \text{ M}^{-1} \text{ cm}^{-1}$ for **3**). Details of the electronic transitions obtained from the DFT calculations are described

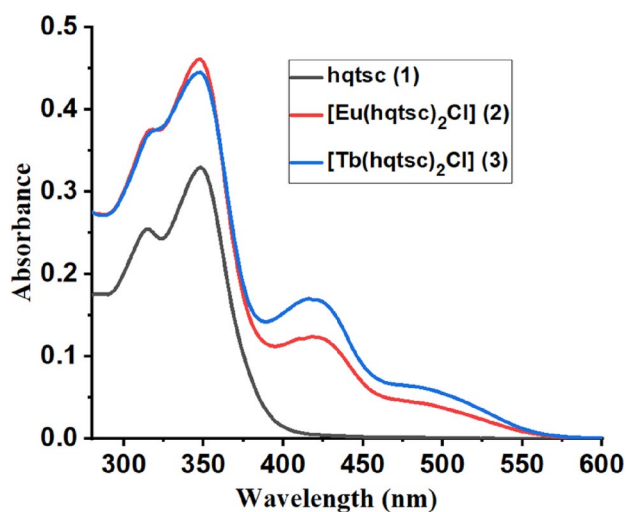


Fig. 1 Electronic absorbance spectra of hqtsc and its trivalent lanthanide (Eu and Tb) complexes in 1×10^{-5} M DMF

in “Theoretical electronic spectra of europium and terbium complexes” section.

Solution thermodynamics

Protonation studies of ligand

The protonation behavior of the ligand was investigated in solution. The potentiometric titrations of the ligand hqtsc (concentration 10^{-3} M) were performed in a highly aqueous solution (9:1, water: DMSO) by adding an excess of standard HCl (0.1 M) and titrating it against a standard KOH (0.1 M) solution. The potentiometric data were analyzed by Hyperquad program, which yielded the best match for three protonation constants with $\log K_1 = 11.89$, $\log K_2 = 9.55$, and $\log K_3 = 3.36$ corresponding to the phenolic -OH, pyridine N, and secondary amine (-NH) group. Four species were formed, namely LH_3^+ , LH_2 , LH^- , and L^{2-} (Fig. 2), across the pH range 3–10. The values of protonation constants are consistent well with the literature [58]. The protonation behavior of hqtsc was also checked through spectrophotometric studies where 30 absorption spectra were taken between 250 and 600 nm in the pH range 2–10. The spectra established the equilibrium between the protonated and deprotonated species. The protonation constants obtained from Hyspec are $\log K_1 = 11.76$, $\log K_2 = 9.52$, and $\log K_3 = 3.30$, which agree with potentiometric results. The spectrophotometric titration curves are shown in Fig. S13.

Complex formation studies

Potentiometric titrations of the ligand hqtsc were performed in the presence of Eu^{3+} and Tb^{3+} ions, maintaining the metal: ligand molar ratio as 1:2 for studying the metal complex

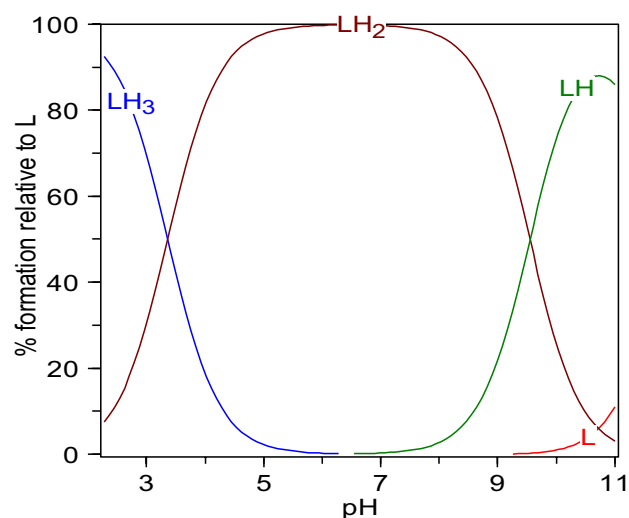


Fig. 2 Species distribution curve for the ligand hqtsc at various pH

formation equilibria. The titrations were done in highly aqueous media (9:1; H₂O: DMSO) having ionic strength $\mu = 0.1\text{MKCl}$ at $25 \pm 1^\circ\text{C}$. The potentiometric curves of metal-ligand systems show deviation from the ligand curve above pH 3.2, suggesting the complex formation (Fig. S14). Different sets of models were considered to get the best-fit data through the global refining program Hyperquad. Complete agreement of the experimental and theoretical curves was obtained when ML_2H_2 , ML_2H_1 , ML_2 , ML_2H_{-1} , and ML_2H_{-2} species were included in the model for both europium and terbium systems. The values of overall formation constants ($\log \beta$) obtained from the calculations are summarized in Table 1, along with the equilibrium reactions.

UV-visible spectroscopy was also used to study the interactions of Eu^{3+} and Tb^{3+} with hqtsc under identical conditions similar to the potentiometric study. The absorption spectra were taken in the pH range from 2 to 11 for both the metal systems in a 1:2 metal-to-ligand ratio and $0.5 \times 10^{-3}\text{ M}$ concentration. The ligand shows two bands at 303 nm and 334 nm due to $\pi \rightarrow \pi^*$ transitions in acidic pH 3.0 to 6.8. Changes in the ligand-based transitions and observation of new bands with increasing pH indicate the formation of complexes (Fig. 3a, b). In the acidic pH range from 3 to 6, the bands at 303 and 334 nm showed a decrease in intensity. At the neutral and basic pH, these two bands (303 nm and 334 nm) merged into a single broad band with λ_{max} at 340 nm, and a new band at 390 nm appeared due to the formation of $\text{EuL}_2\text{H}_{-1}$ species. Similarly, in the case of the Tb^{3+} system, there was a decrease in the intensity of the ligand band at 303 nm and 334 nm, along with the observation of a new band at 398 nm due to the formation of $\text{TbL}_2\text{H}_{-1}$. Above neutral pH, two new absorption bands at ~ 340 and 390 nm appeared due to the existence of $\text{TbL}_2\text{H}_{-2}$. The best-fit model on the global refining program Hyspec gave results similar to those obtained from potentiometric data. The outcomes are listed in Table 1. Figure 3c and d

shows the spectrum of individual species calculated from the Hyspec program.

The species distribution curves for the complex formation obtained from the potentiometric titrations are given in Figure 4. It can be seen that in acidic pH, species EuL_2H_2 and EuL_2H form for europium. Initially, the EuL_2H_2 exists in significant quantity, i.e., 98% around pH 2.5, and EuL_2H exists with a maximum of 45% at pH 4. With the increase in pH, deprotonation of the secondary $-\text{NH}$ group of thiosemicarbazone moiety will lead to simultaneous coordination with the metal ion, leading to the formation of EuL_2 species. The EuL_2 species formed around pH ~ 3 and existed at a maximum concentration of 82% at pH ~ 5.0 . The hydrolysis species formation started above pH ~ 5 . $\text{EuL}_2\text{H}_{-1}$ presents a maximum of 38% at pH 6.5, whereas $\text{EuL}_2\text{H}_{-2}$ exists in 100% at pH > 9 . In the case of terbium, TbL_2H_2 and TbL_2H formed with 98% and 65% at pH 2 and 4, respectively. The TbL_2 species formation occurred around pH ~ 3 and was found a maximum of 75% at pH 5.3. The hydrolysis species $\text{TbL}_2\text{H}_{-1}$ and $\text{TbL}_2\text{H}_{-2}$ are 45% and 100% at pH 6.4 and > 8.5 , respectively.

Anion sensing

Visual detection of anions

The anion sensing asset of the two lanthanide complexes $\text{Eu}(\text{hqtsc})_2\text{Cl}$ (**2**) and $\text{Tb}(\text{hqtsc})_2\text{Cl}$ (**3**) was examined considering various anions such as F^- , Cl^- , Br^- , H_2PO_4^- , HSO_4^- , I^- , ClO_4^- , CN^- , BF_4^- , PF_6^- and S^{2-} in DMF solution. After adding three equivalents of these anions into the solution of complexes **2** and **3**, both showed a prominent change in color with only H_2PO_4^- and CN^- . In the presence of H_2PO_4^- ions, complex **2** changed from orange to colorless, and the yellow solution **3** became colorless. However, both complexes turned dark red with the CN^- ions. Such

Table 1 The values of $\text{Log } \beta$ obtained through potentiometric and spectrophotometric titrations along with the equilibrium reactions involved

Equilibrium reaction	Expression for $\log \beta$	Poten-tiometric $\log \beta$	Spectropho-tometric $\log \beta$	Average ($\text{Log } \beta$)
[Eu(hqtsc)₂]				
$\text{Eu} + 2\text{L} \rightleftharpoons \text{EuL}_2$	$[\text{EuL}_2]/[\text{Eu}][\text{L}]^2$	26.57	26.54	26.55 ± 0.02
$\text{Eu} + 2\text{L} + \text{H} \rightleftharpoons \text{EuL}_2\text{H}$	$[\text{EuL}_2\text{H}]/[\text{Eu}][\text{L}]^2[\text{H}]$	31.43	31.49	31.44 ± 0.04
$\text{Eu} + 2\text{L} + 2\text{H} \rightleftharpoons \text{EuL}_2\text{H}_2$	$[\text{EuL}_2\text{H}_2]/[\text{Eu}][\text{L}]^2[\text{H}]^2$	34.95	34.97	34.96 ± 0.01
$\text{Eu} + 2\text{L} \rightleftharpoons \text{EuL}_2\text{H}_{-1} + \text{H}$	$[\text{EuL}_2\text{H}_{-1}][\text{H}]/[\text{Eu}][\text{L}]^2$	20.18	20.12	20.15 ± 0.04
$\text{Eu} + 2\text{L} \rightleftharpoons \text{EuL}_2\text{H}_{-2} + 2\text{H}$	$[\text{EuL}_2\text{H}_{-2}][\text{H}]^2/[\text{Eu}][\text{L}]^2$	13.95	13.99	13.97 ± 0.01
[Tb(hqtsc)₂]				
$\text{Tb} + 2\text{L} \rightleftharpoons \text{TbL}_2$	$[\text{TbL}_2]/[\text{Tb}][\text{L}]^2$	27.16	27.11	27.13 ± 0.04
$\text{Tb} + 2\text{L} + \text{H} \rightleftharpoons \text{TbL}_2\text{H}$	$[\text{TbL}_2\text{H}]/[\text{Tb}][\text{L}]^2[\text{H}]$	31.32	31.36	31.34 ± 0.02
$\text{Tb} + 2\text{L} + 2\text{H} \rightleftharpoons \text{TbL}_2\text{H}_2$	$[\text{TbL}_2\text{H}_2]/[\text{Tb}][\text{L}]^2[\text{H}]^2$	35.21	35.28	35.24 ± 0.04
$\text{Tb} + 2\text{L} \rightleftharpoons \text{TbL}_2\text{H}_{-1} + \text{H}$	$[\text{TbL}_2\text{H}_{-1}][\text{H}]/[\text{Tb}][\text{L}]^2$	21.05	21.07	21.06 ± 0.01
$\text{Tb} + 2\text{L} \rightleftharpoons \text{TbL}_2\text{H}_{-2} + 2\text{H}$	$[\text{TbL}_2\text{H}_{-2}][\text{H}]^2/[\text{Tb}][\text{L}]^2$	14.24	14.28	14.26 ± 0.02

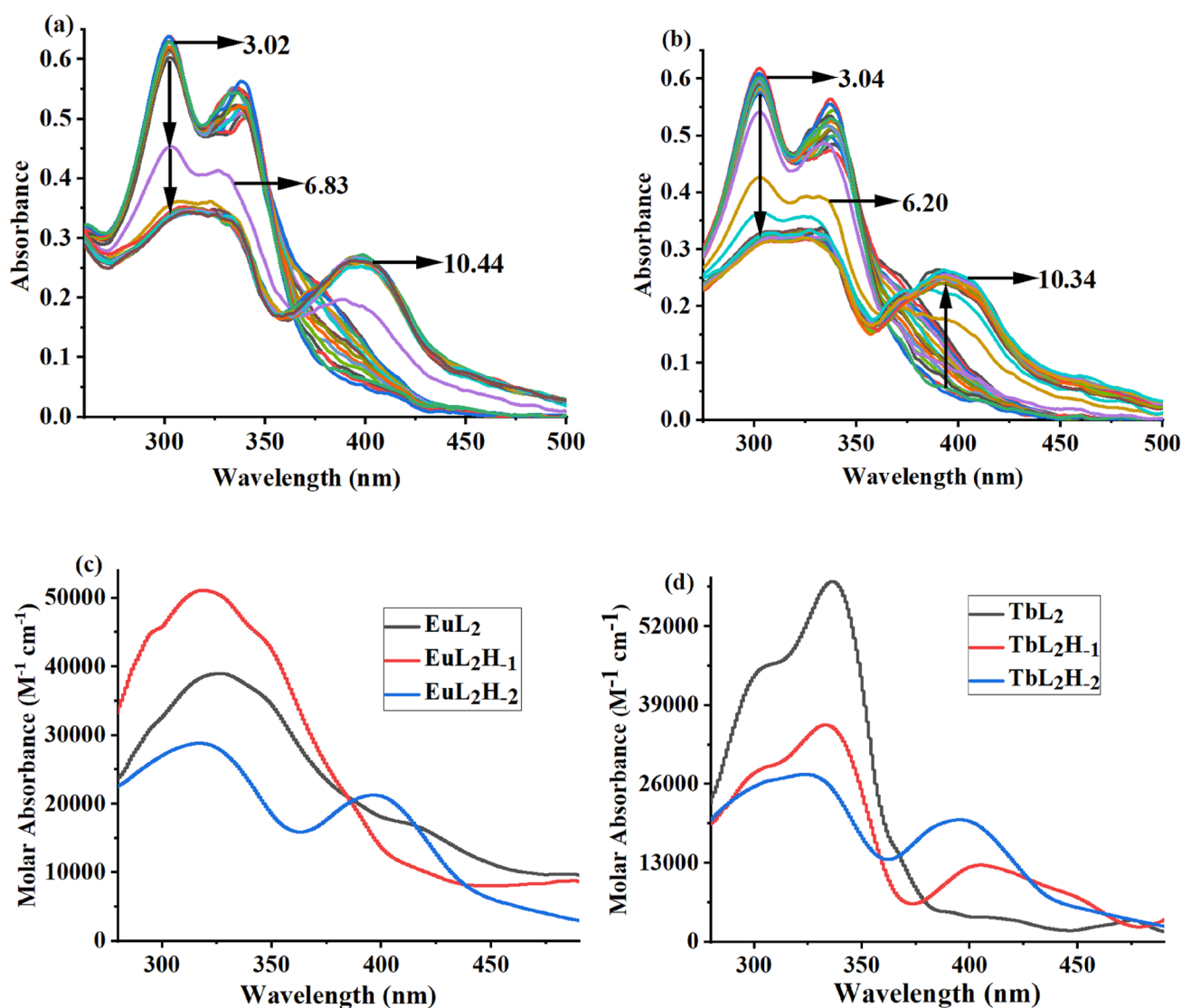


Fig. 3 Experimental electronic absorption spectra of hqtsc at various pH in the presence of **a** Eu³⁺ and **b** Tb³⁺; Absorption spectra of the species obtained from Hyspec for (c) Eu³⁺ and (d) Tb³⁺

instantaneous changes in color due to the interaction of anions demonstrate that the complexes can be explored as potential probes for the naked-eye sensing and detection of H₂PO₄⁻ and CN⁻ colorimetrically. The color of complexes **2** and **3** in the presence of different anions in DMF solution is displayed in Figure 5a and b.

Changes in absorption spectra in the presence of anions

Based on the preliminary observations regarding sensing two anions (H₂PO₄⁻ and CN⁻) by Eu-hqtsc and Tb-hqtsc complexes via spectral and color changes, further studies were undertaken to shed light on the sensing mechanism and selectivity for the ions. The electronic absorption spectra of probes **2** and **3** were recorded in DMF medium,

which displayed four bands at 314 nm, 346 nm, 418 nm, and 490 nm. The addition of one equivalent of H₂PO₄⁻ ions resulted in noticeable changes in the spectra of both probes. A 1.5-fold and 1.4-fold enhancement in the absorbance of the band at 346 nm was noticed for **2** and **3**, respectively, along with an increase in the absorbance of the band at 314 nm. Also, in both cases, the bands at 418 nm and 490 nm were wholly quenched in the presence of H₂PO₄⁻ ions. Such changes in the absorption spectra are responsible for the change in color from orange (**2**) and yellow (**3**) to colorless. However, with the addition of one equivalent of CN⁻, the spectral changes were not very distinct. Still, adding three equivalents resulted in observable spectral changes in both complexes and the bands at 314 nm and 346 nm disappeared with the appearance of a new band at 342 nm, which was

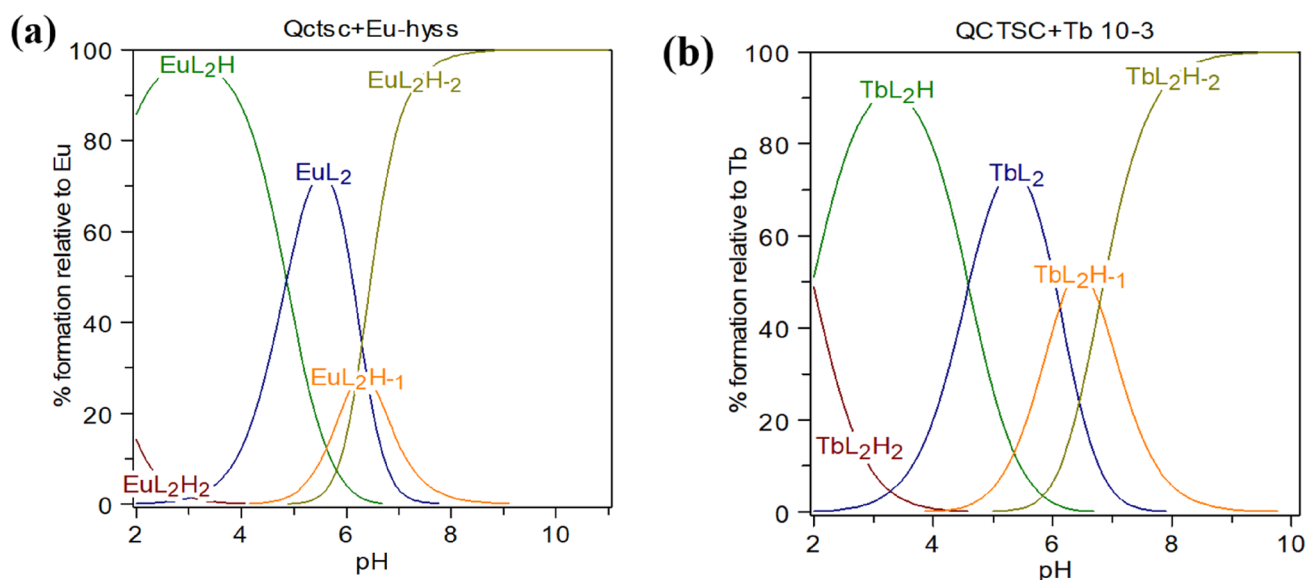


Fig. 4 The pH-dependent species distribution curve of Ln^{3+} complexes **a** Eu-hqtsc and **b** Tb-hqtsc

(a)



(b)



Fig. 5 Colour change in complexes (1×10^{-4} M) in the presence of anions (3×10^{-4} M) in DMF: **a** Eu-hqtsc and **b** Tb-hqtsc

much lower in absorbance (0.57 for **2** and 0.54 for **3**). Moreover, an appreciable increase in absorbance of transitions at 418 nm and 490 nm was also observed in both cases. These

changes are responsible for the intensification of color from orange (**2**) / yellow (**3**) to red, which can be observed with the naked eye. The addition of other anions mentioned above

did not show any noticeable changes in the absorption spectra of either probe, even up to 5 equivalents of the addition of the ions. Figure 6a and b show the absorption spectra of complexes **2** or **3** in the presence of different anions.

For an in-depth understanding of the binding properties of **2** and **3** towards H_2PO_4^- and CN^- , UV-Vis spectral titrations were carried out in DMF. As shown in Figure 7a and b, incremental addition of H_2PO_4^- ions into the solution of **2** and **3**, respectively, depicted a continuous increase in absorbance of the bands at 314 nm and 346 nm while the absorbance at 418 nm and 490 nm decreased continuously with a clear isosbestic point at 380 nm.

The absorption spectra attained saturation after adding one equivalent (0–20 μM) of H_2PO_4^- ions, suggesting a 1:1 stoichiometric ratio of H_2PO_4^- ions with complexes **2** and **3** and are also confirmed by Job's plot method (Fig. 8a, b). The binding constants of complexes **2** and **3** with H_2PO_4^- ions were calculated from the titration data using B–H plots. The values are found to be $9.09 \times 10^3 \text{ M}^{-1}$ and $6.32 \times 10^3 \text{ M}^{-1}$ for **2** and **3**, respectively. The limit of detection (LOD) for the dihydrogen phosphate ions was calculated by plotting Absorbance (A/A_0) against increasing concentrations of H_2PO_4^- ions in both cases and found to be $7.6 \times 10^{-6} \text{ M}$ and $6.3 \times 10^{-6} \text{ M}$ respectively, using equation $\text{LOD} = 3\sigma/S$,

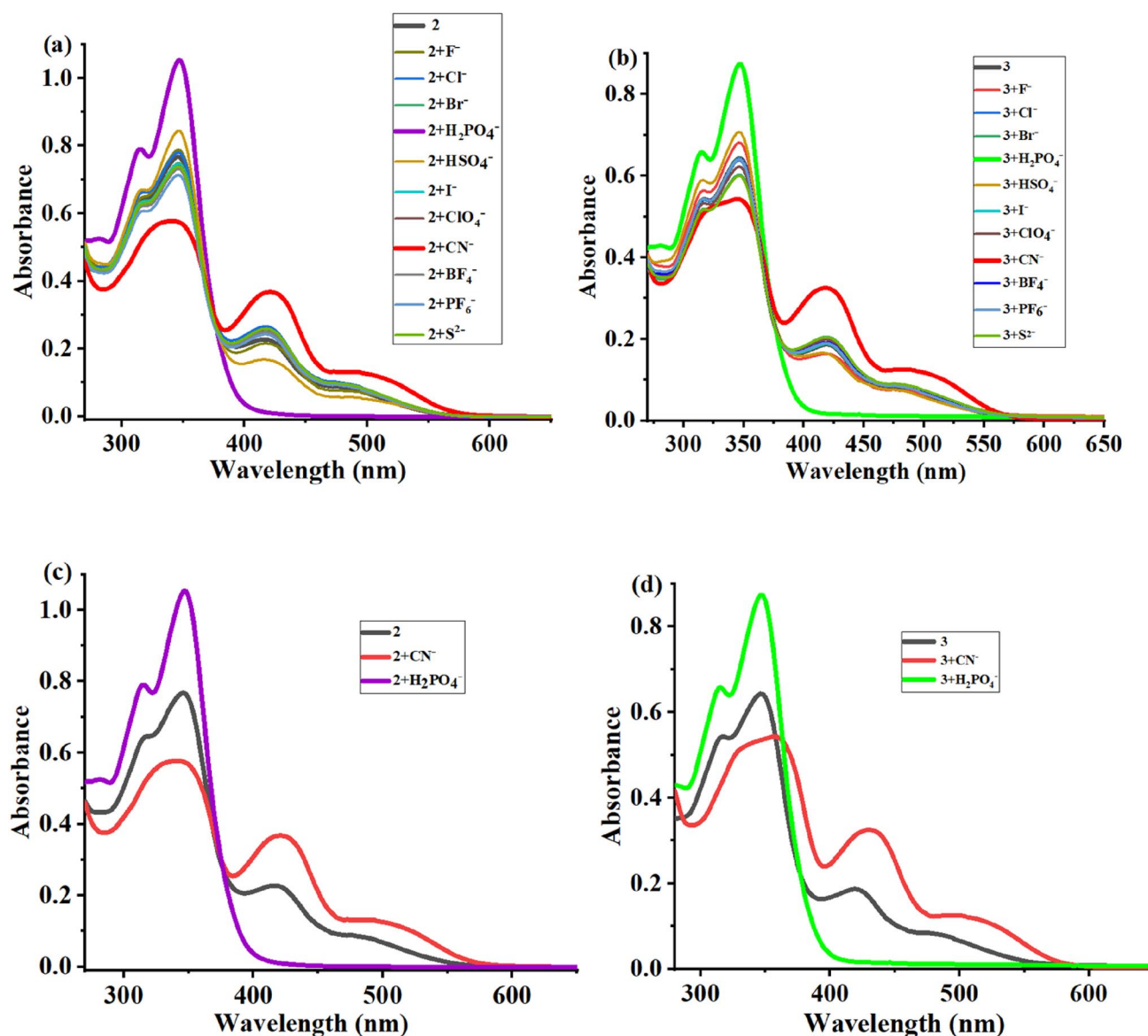


Fig. 6 a UV-Vis absorbance spectra of complexes ($0.2 \times 10^{-4} \text{ M}$) in the presence of different anions ($0.6 \times 10^{-4} \text{ M}$) in DMF medium a $\text{Eu}(\text{hqtsc})_2\text{Cl}$; b $\text{Tb}(\text{hqtsc})_2\text{Cl}$; c complex **2** with H_2PO_4^- and CN^- ; d complex **3** with H_2PO_4^- and CN^-

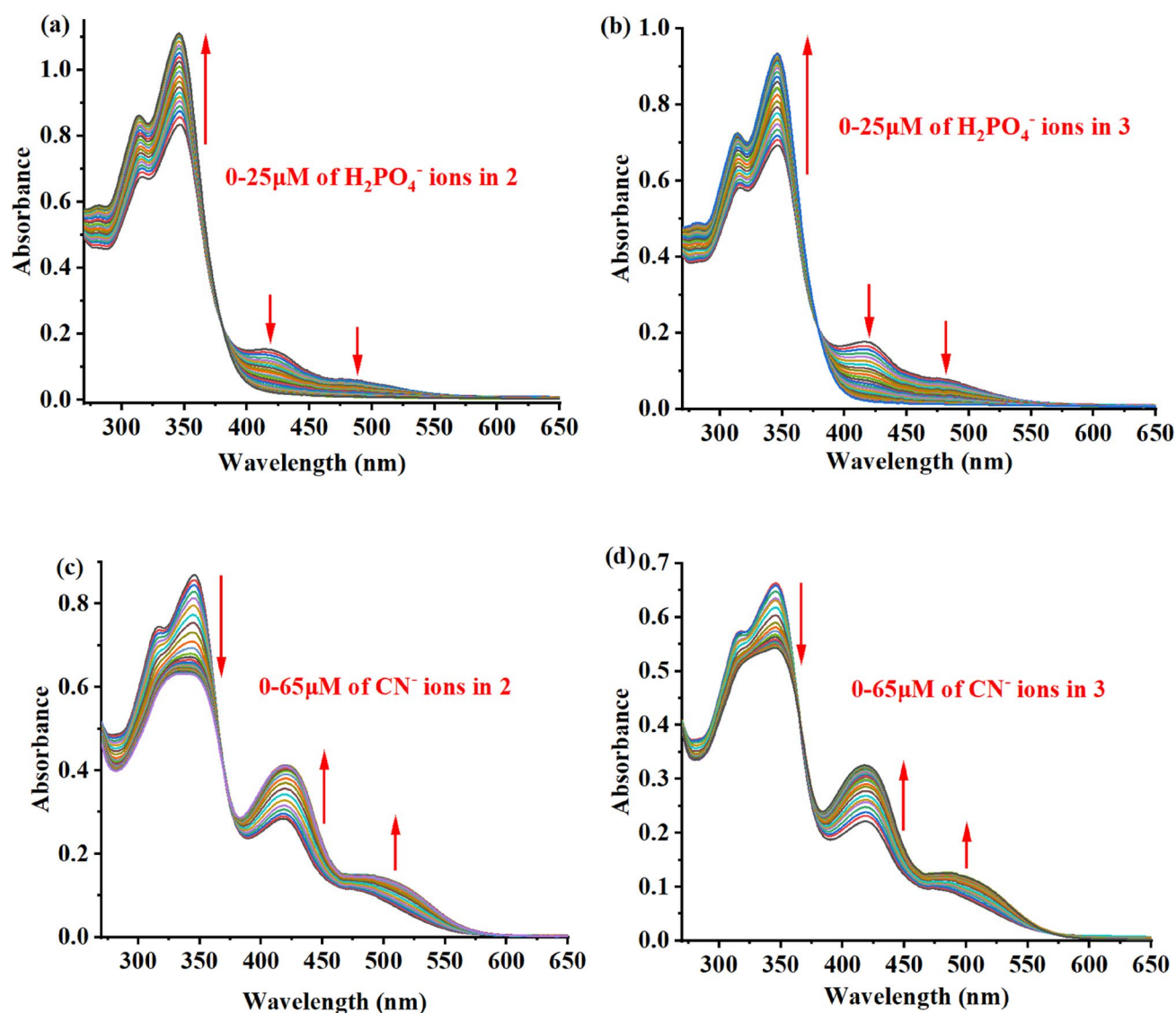


Fig. 7 Absorbance titration of probes (20 μM) upon addition of H_2PO_4^- (0–25 μM) in DMF: **a** 2, **b** 3. Absorbance titration of probes (20 μM) upon addition of CN^- (0–65 μM) in DMF **c** 2, **d** 3

where σ is the standard deviation of the blank solution, and S is the slope of the titration plot.

The probes showed completely different absorption spectra in the presence of CN^- ions compared to H_2PO_4^- ions. Experiments were performed by incremental addition of CN^- ions to the probes. A continuous decrease in the intensity of the bands at 314 nm and 346 nm occurred till 20 μM (1:1). Above that, a completely new band appeared at 342 nm (Fig. 7c, d). The new band also showed a decrease in the intensity up to 60 μM (1:3), after which saturation was attained. A prominent isosbestic point was observed at 368 nm in both cases. In addition to the above observation, the bands at 416 nm and 480 nm showed an increase in the absorbance, and saturation was

achieved in the absorbance after adding three equivalents (0–60 μM) of CN^- ions, signifying a 1:3 stoichiometry binding of cyanide ions which was further confirmed by Job's plot. The detection limits evaluated towards CN^- for complexes 2 and 3 are 12 μM and 18 μM (Fig. 9c, d), and the respective binding constants calculated using Benesi Hildebrand plot (Fig. 10c, d), are $2.32 \times 10^3 \text{ M}^{-1}$ and $2.47 \times 10^3 \text{ M}^{-1}$, respectively.

The observed LOD values and binding constants indicate high selectivity and strong binding of both complexes towards H_2PO_4^- and CN^- anions. The formation of a single isosbestic point in all four cases suggests that only two species, i.e., probe and anion-probe adduct, co-exist in the solution.

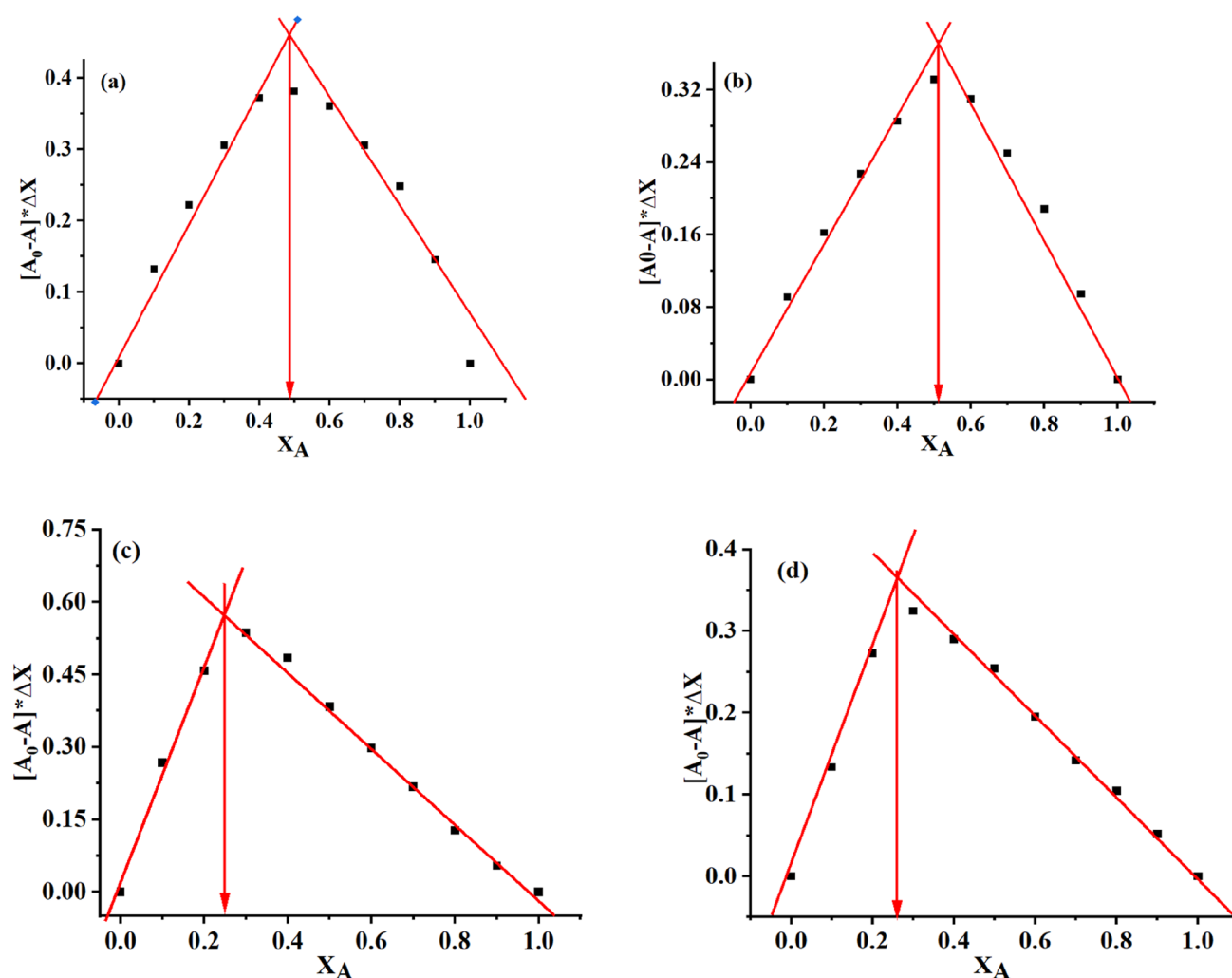


Fig. 8 Job's plot for determination of the stoichiometric ratio of **a** 2 with H_2PO_4^- ions; **b** 3 with H_2PO_4^- ions; **c** 2 with CN^- ions; **d** 3 with CN^- ions

Binding mechanism

The appearance of different colors and completely different spectra in the presence of H_2PO_4^- and CN^- suggests that probes **2** and **3** can simultaneously detect dihydrogen phosphate and cyanide ions. It can also be inferred that both the anions have different binding mechanisms towards the complexes. After adding H_2PO_4^- ions to **2** and **3**, the chloride present in the complexes was replaced by dihydrogen phosphate as it is a more potent donor than chloride ion (Scheme 2), subsequently changing the color and spectral behavior of the optical probes [59]. DFT calculations (“Theoretical electronic spectra of europium and terbium complexes” section) revealed that in the visible region the transition involved some percent of chloride to vacant ligand orbitals in the complexes, which disappeared when the replacement of Cl^- by H_2PO_4^- ions occurred.

Obviously, a new adduct $\text{Ln}(\text{hqtsc})_2\text{-H}_2\text{PO}_4^-$ formed in the process that showed different spectral behavior and color.

Experimental results of Job's plot method showed that cyanide ions bind with the probes in a 1:3 ratio. The binding of three CN^- can be explained due to the replacement of only one available Cl^- by CN^- , and the bonding of remaining two CN^- ions to the two functional secondary $-\text{NH}$ groups. The colorimetric and spectral changes observed in the case of cyanide ions suggest that two CN^- ions extract the proton from the secondary $\text{NH}-$ groups of the thiosemicarbazone moiety from both the ligands resulting in the deprotonated complexes (Scheme 3). As a result, the new adduct $[\text{Ln}(\text{hqtsc})_2\text{CN}]^{2-}$ formed that showed color changes and enhancement in absorbance of the band at 418 and 490 nm along with a new band at 342 nm.

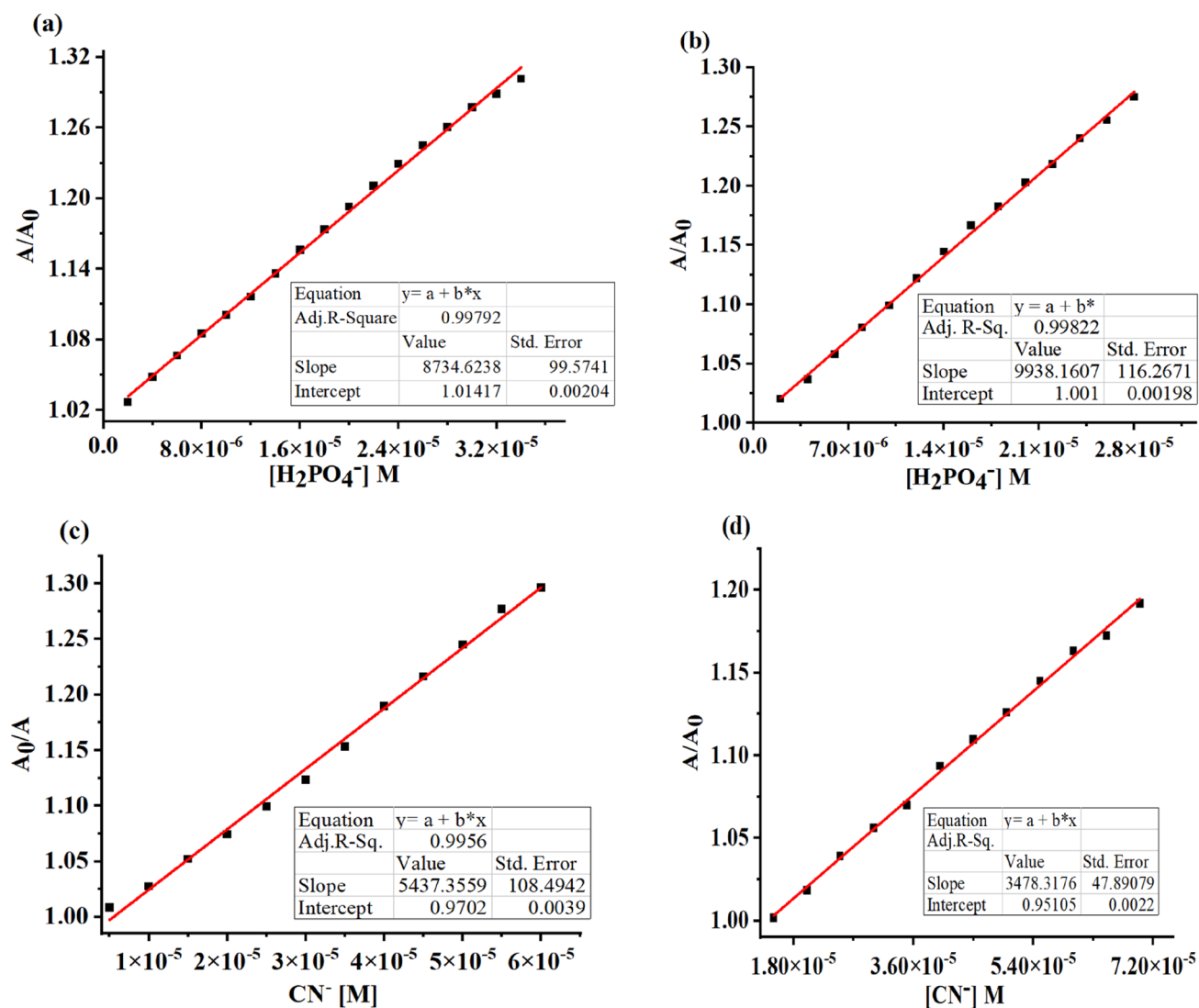


Fig. 9 The linear relationship plot for calculating the detection limit with the increase in concentration of **a** $H_2PO_4^-$ vs. **2**; **b** $H_2PO_4^-$ vs. **3** CN^- vs. **2**; **d** CN^- vs. **3**

Emission spectra

The emission behavior of the complexes were studied in DMF by exciting them at 418 nm. The emission spectra of both the complexes in presence of $H_2PO_4^-$ and CN^- ions were also measured (Fig. S22a, b). The complexes **2** and **3** showed poor emission at 837 nm with intensities 1.24 a.u. and 2.96 a.u., respectively. On adding $H_2PO_4^-$ ions, the emission intensities were increased by ~ 2-fold in each case. In the presence of CN^- ions, complex **2** showed quenching in the emission from 1.24 a.u. to 0.73 a.u., whereas in complex **3** the emission intensity increased slightly (3.36 a.u.) along with a red shift from 837 to 849 nm. It is concluded that the anions $H_2PO_4^-$ and CN^- can be detected through emission studies; however,

the changes in intensities of emissions are not that prominent as observed in the absorbance spectroscopy.

In-silico studies

To have a deep understanding of the molecular structures, bonding, spectral properties, and sensing mechanism of the ligand and two synthesized lanthanide complexes, theoretical studies were performed at the DFT level.

Geometry prediction

The ligand hqtsc possesses five rotatable bonds and one imine (C=N) bond, which are accountable for the presence

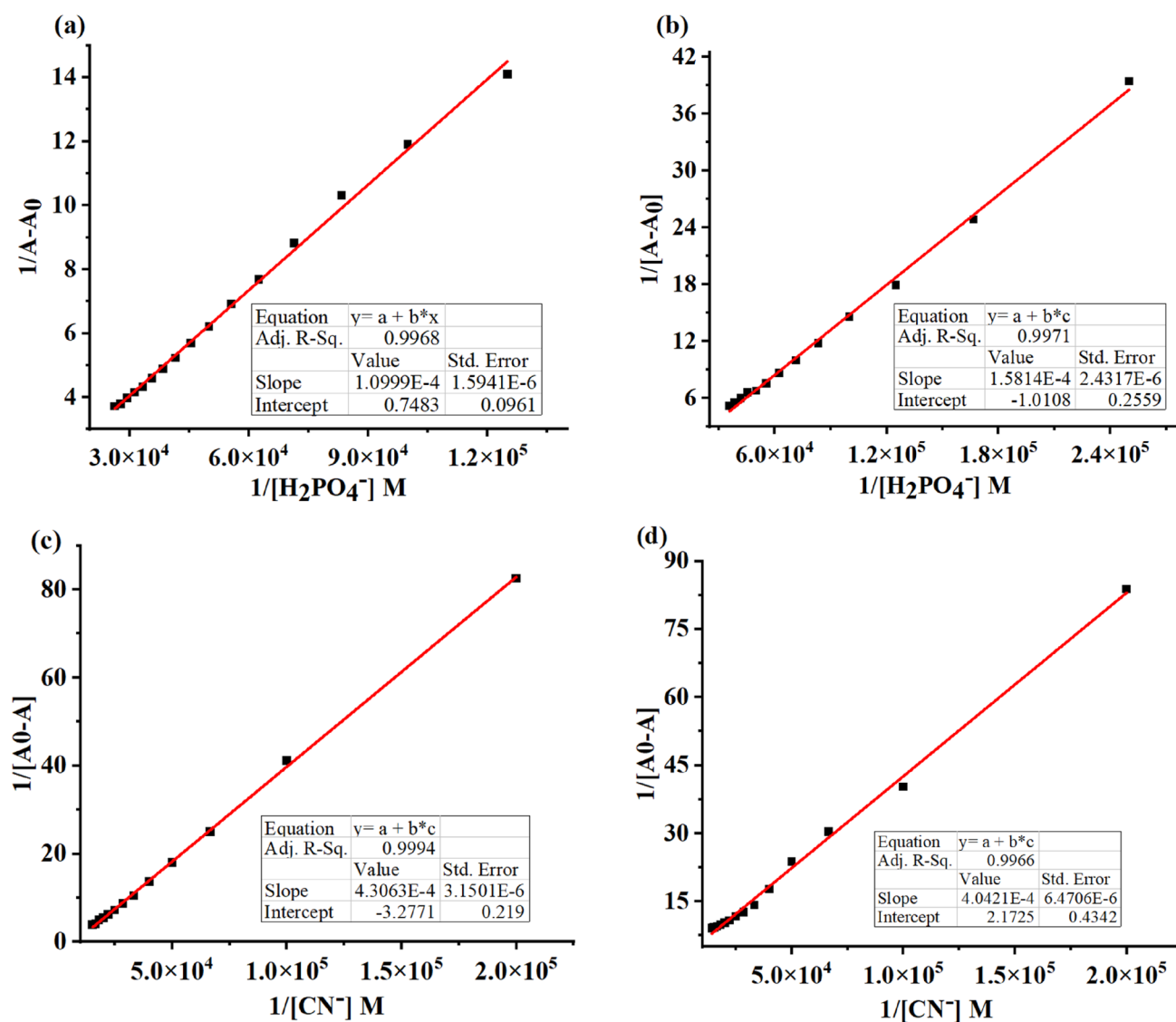
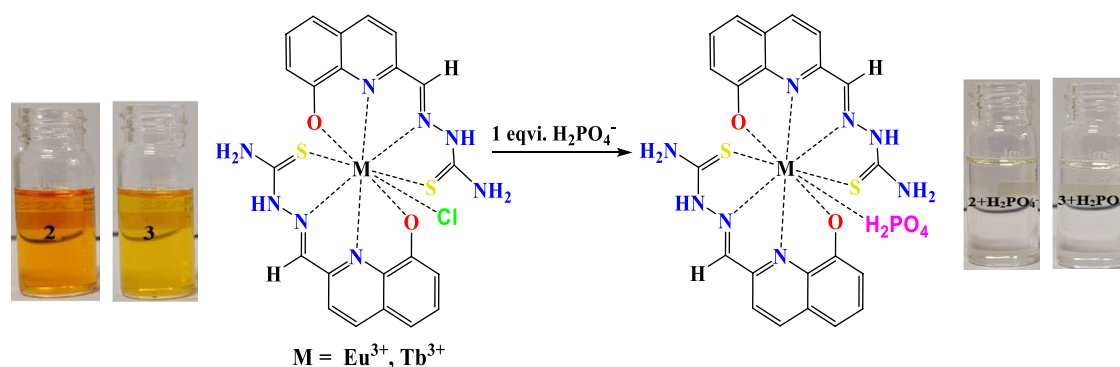
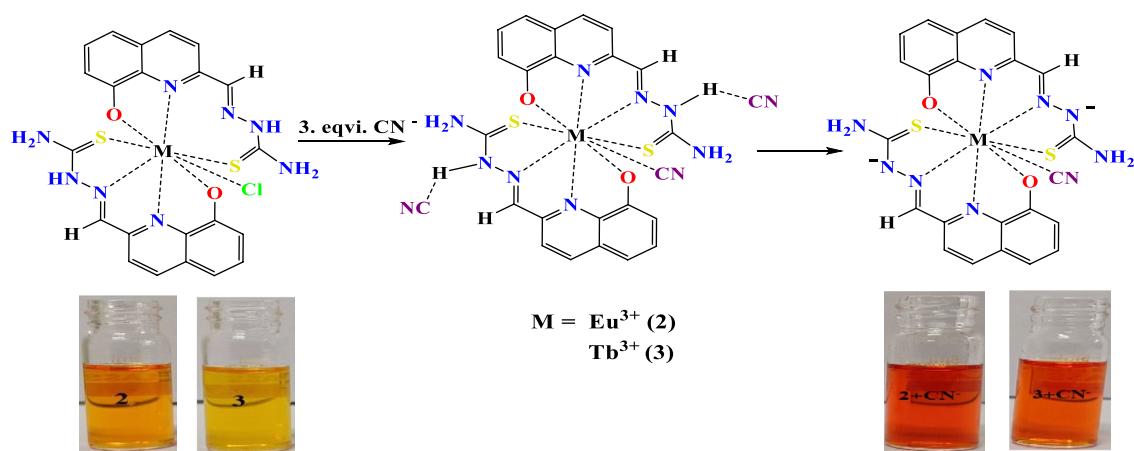


Fig. 10 Benesi–Hildebrand curve for calculating binding constant of **a** 2 with H_2PO_4^- ; **b** 3 with H_2PO_4^- ; **c** 2 with CN^- ; **d** 3 with CN^-



Scheme 2 Mechanism of sensing H_2PO_4^-



Scheme 3 Mechanism of sensing CN^- ions by complexes **2** and **3**

of E and Z isomers. Both the isomers were built and tested for the presence of the lowest energy conformer. From the conformational energy analysis, the E form was found to have the lower energy than Z form. The E-form of the ligand was then optimized at DFT level using BLYPD3/DZ basis set, and the optimized structure (Fig. S15a) thus obtained is identical to that of the single-crystallographic research [54]. The geometric parameters, i.e. bond distances and bond angles, are also comparable details which are given in Table S1. The ligand possesses six donor atoms, i.e. one O, four N, and one S, and can bind to the metal ions through two possible tetradentate binding modes, i.e., (N, N, N, O) or (N, N, O, S). Preliminary calculations at the molecular mechanics level indicated that the N, N, O, S type of coordination mode is energetically more favorable where one N atom is from the hydroxyquinoline group and the other from the imine bond ($-\text{C}=\text{N}-$). The coordination number of lanthanides range from six to twelve. However, for Eu^{3+} and Tb^{3+} , coordination numbers 8 and 9 are the most common. Accordingly, two structures were proposed for the lanthanide complexes: $[\text{Ln}(\text{hqtsc})_2]^+$ having eight coordination and $\text{Ln}(\text{hqtsc})_2\text{Cl}$ (Ln is $\text{Eu}^{3+}/\text{Tb}^{3+}$) with nine coordinated structures. Both the proposed structures were optimized through molecular mechanics. The results suggest that the neutral structures having nine-coordinated geometry are more stable with minimum strain energies than the eight-coordination structures carrying a positive charge. Therefore, the complexes are presented as nine-coordinated structures with formulations $\text{Eu}(\text{hqtsc})_2\text{Cl}$ (**2**) and $\text{Tb}(\text{hqtsc})_2\text{Cl}$ (**3**). The stoichiometry has also been confirmed from the experimental results.

The resulting structures were then optimized by the Sparkle model. The sparkle model is an effective tool for the optimisation of lanthanide complexes due to its low processing cost and gives similar outcomes as the

high-level quantum mechanics calculations. The geometry from the sparkle model was then further optimized in the gas phase at a DFT level using BLYPD3 functional and DZ basis sets for the Eu-complex and BP86/DZ for the Tb-complex. The optimized structures of complexes **2** and **3** are displayed in Fig. 11. The geometry around the Eu^{3+} and Tb^{3+} metal centers may be defined as distorted tricapped trigonal prism (Fig. 11b, e). From the optimized structures of complexes **2** and **3**, it can be seen that the hydroxyquinoline rings of both the ligands bend towards the $\text{M}-\text{Cl}$ bond, giving a butterfly like appearance (Fig. 11c, f). In the case of complex **3** the hydroxyquinoline rings are slightly more bent towards the $\text{M}-\text{Cl}$ bond than complex **2**. The $\text{M}-\text{S}$ bonds are elongated one and present above the wings of seemingly butterfly formed by hydroxyquinoline rings. The geometric parameters of both complexes are given in SI (Table S2).

DFT predicted IR of Ln^{3+} complexes

The theoretical IR data was obtained under the same DFT level as the optimization, and compared it with the experimental data (Table 2), the slight difference in calculated and experimental values is because the experimental spectra were taken in solid phase, whereas computational frequency analysis is done in gaseous phase. Each complex molecules contains 55 atoms, and therefore, 159 frequencies are predicted. The ligand hqtsc is projected to have 75 peaks corresponding to 27 atoms. Figures S17–S19 depict the theoretical IR spectra of hqtsc and the complexes. Figure 12a and b shows the regression analysis plots of complexes **2** and **3**, respectively, with acceptable correlation factor (R^2).

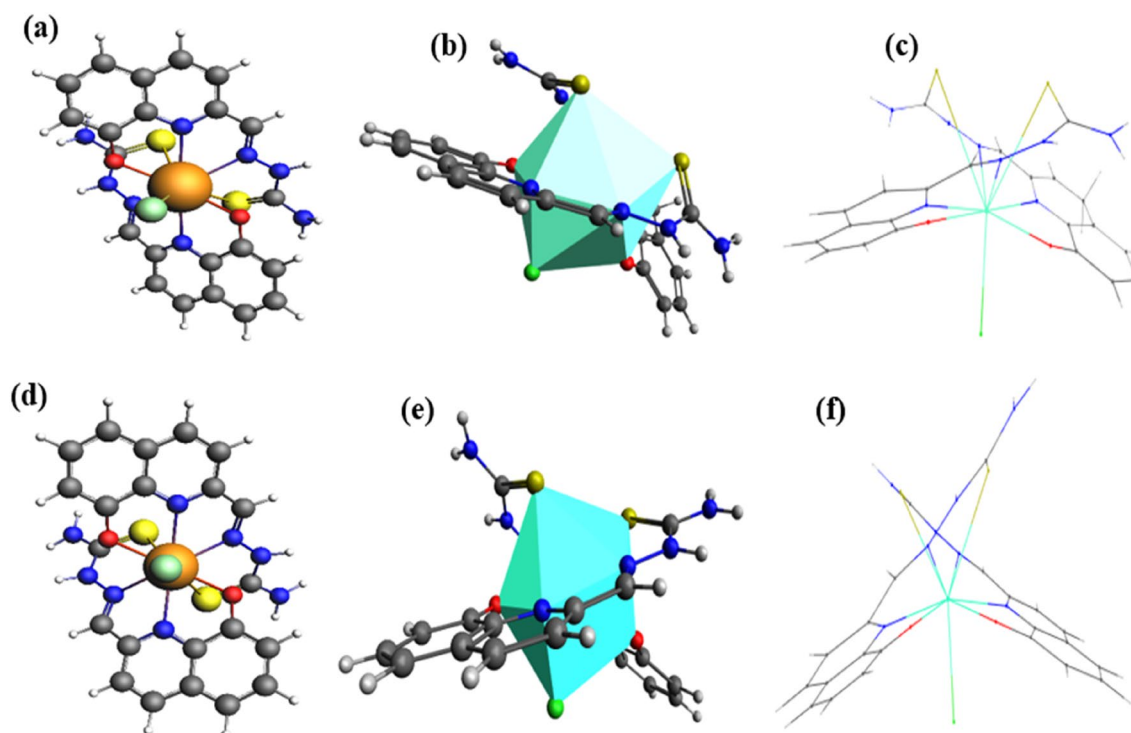


Fig. 11 DFT optimized structure of **a** complex **2**; **d** complex **3** (ball and stick model). Polyhedron with distorted tricapped trigonal prismatic geometry of **b 2**; **e 3**– Butterfly appearance, **c 2**; **f 3**

Table 2 Comparison of calculated (GGA-BLYP-D3 for complex **2** and GGA-BP86 for complex **3**) and experimental (KBr pallet) IR frequencies

Functional group	Eu(hqtsc) ₂ Cl		Tb(hqtsc) ₂ Cl	
	Experimental (cm ⁻¹)	Theoretical (cm ⁻¹)	Experimental (cm ⁻¹)	Experimental (cm ⁻¹)
νSecondaryN–H	3161	3347	3163	3373
νNH ₂ (bending)	1597	1635	1616	1630
νC=N	1535	1540	1535	1560
νC=S	1273	1270	1271	1261
νC–O	1330	1326	1330	1326
νN–N	1058	1060	1049	1083
νM–N	495	510	497	507
νM–O	439	425	441	446

Theoretical electronic spectra of europium and terbium complexes

The theoretical computations were used to establish the absorption spectra of hqtsc in the gas phase at the TD-DFT level using MODEL SAOP with bandwidth 30. From the theoretical absorption spectrum of hqtsc, two prominent peaks at 300 and 346 nm having oscillator strengths of 0.4107 and 0.3891 were identified, which were in close

agreement with experimental spectra (Fig. S20). Both the ligand transitions are considered as $\pi \rightarrow \pi^*$ transitions. The frontier orbitals involved in the electronic transitions of the ligand are represented in Table S3.

The theoretical absorption spectra of complexes were initially predicted using ZINDO/s at CIS level in Orca where the lanthanide ion is replaced by +3e point charge. The theoretical transitions obtained were in good correlation with the experiment values with zero offset. The electronic spectra of the complexes were also calculated at the TD-DFT level using GGA/PBE functional and DZ basis set. The offset values for Eu(hqtsc)₂Cl and Tb(hqtsc)₂Cl were – 690 and – 670 nm, respectively, and the bandwidth was set as 15 in both the cases to match the theoretical spectra with the experimental one (Fig. 13). A comparison of the results from the ZINDO/s and TD-DFT calculations with the experimental results is given in Table 3. The theoretical electronic spectra of complexes obtained from TD-DFT calculations show four absorption bands. For Eu-complex, the transitions at 317 nm, 341 nm, 384 nm, and 410 nm correspond with oscillator strengths 0.0009, 0.0026, 0.0002 and 0.0004, respectively, whereas in the case of Tb-complex, the spectral bands at 317 nm, 365 nm, 398 nm and 444 nm with oscillator strength 0.0008, 0.0012, 0.0003 and 0.0001 respectively were obtained at the DFT. As depicted in Fig. 13a and b, the theoretical results differ slightly

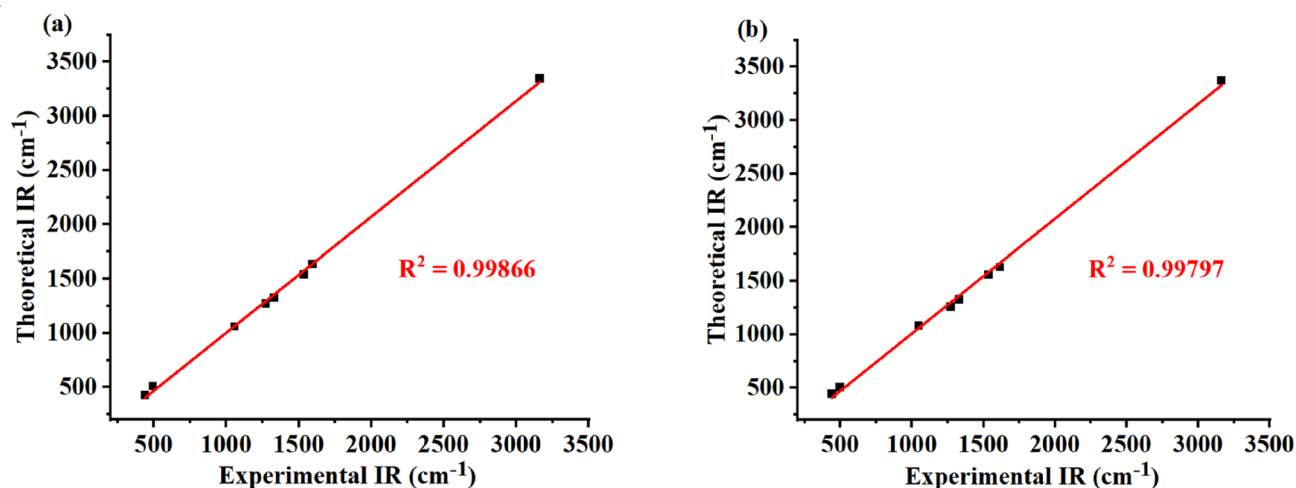


Fig. 12 Correlation of experimental and theoretical IR a complex 2; b complex 3

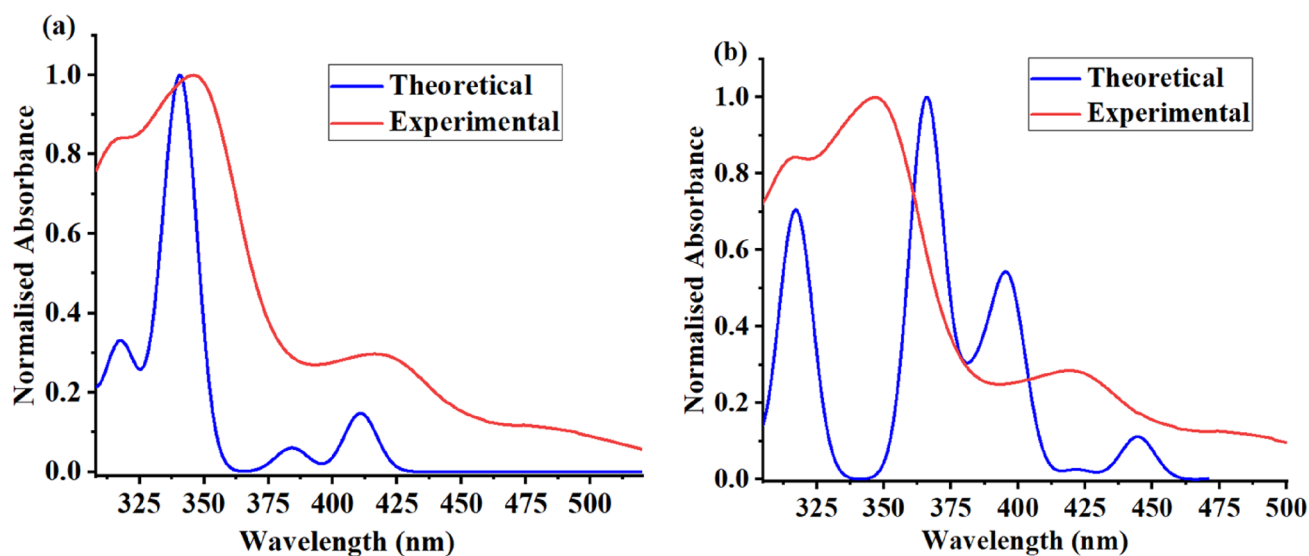


Fig. 13 Theoretical (gas phase, at DFT level) and experimental (DMF, 0.2×10^{-4} M) electronic spectra of a complex 2; b complex 3

Table 3 Comparison of experimental and calculated (ZINDO/s and GGA/PBE) electronic transitions

S. no.	Experimental (DMF) For both complexes	Theoretical ZINDO/s		Theoretical GGA/PBE/DZ	
		Eu(hqtsc) ₂ Cl (no offset)	Tb(hqtsc) ₂ Cl (no offset)	Eu(hqtsc) ₂ Cl (offset – 690)	Tb(hqtsc) ₂ Cl (offset – 670)
1.	314	293	331	317	317
2.	346	342	349	341	365
3.	418	496	526	384	398
4.	490	516	567	410	444

from experimental electronic spectra of Eu(hqtsc)₂Cl and Tb(hqtsc)₂Cl exhibiting four bands at 314, 346, 418, and 490 nm each; this difference can be explained on the basis of the fact that experimental studies were done in DMF medium

whereas theoretical calculations carried out in the gaseous phase in different functionals and basis sets.

In the case of the europium complex, the band at 317 nm occurs due to the transition from (HOMO) to LUMO+4 with

63.8% contribution and 18.9% contribution from HOMO-21 \rightarrow LUMO. The high energy transition at 341 nm is due to HOMO-19 \rightarrow LUMO (56.6%) and HOMO-21 \rightarrow LUMO (16.5%). The third band at 384 nm occurs due to HOMO-1 \rightarrow LUMO+2 (67.9%) and HOMO-3 \rightarrow LUMO+1 (22.3%). The fourth transition at 410 nm involves a major contribution from HOMO \rightarrow LUMO+2, i.e., 90.1%. In the case of the terbium complex, the transition at 317 nm is due to the 61.9% contribution of HOMO-4 \rightarrow LUMO+3. The second transition at 365 nm, having the highest oscillator strength, is due to a 59.1% contribution from HOMO-1 \rightarrow LUMO+6 and a 38.8% contribution from HOMO-4 \rightarrow LUMO+1. The third band at 398 nm involves transitions due to HOMO-3 \rightarrow LUMO+2 (33.6%) and HOMO-2 \rightarrow LUMO+4 (27.6%). The fourth band at 444 nm

has minimum energy due to HOMO-2 \rightarrow LUMO+4 (32.6%) and HOMO-4 \rightarrow LUMO+1 (30.2%) (Tables 4, 5).

Sensing mechanism through DFT

To further establish the anion sensing mechanism of the complexes towards dihydrogen-phosphate and cyanide ions, geometry optimization of Eu^{3+} and Tb^{3+} anion complexes was done at the DFT level using GGA-BLYPD3-DZ and GGA-BP86-DZ functionals respectively. In the case of complex **2**, the total binding energy obtained after optimization of $\text{Eu}(\text{hqtsc})_2\text{Cl}$ is -330.69 eV, whereas for $\text{Eu}(\text{hqtsc})_2\text{-H}_2\text{PO}_4$ it is -359.66 eV and for $\text{Eu}(\text{hqtsc})_2\text{-CN}$ it is -339.05 eV. In complex **3**, the total binding energy for $\text{Tb}(\text{hqtsc})_2\text{Cl}$ is -342.27 eV, for

Table 4 Most probable transitions involved in the absorption spectra of $\text{Eu}(\text{hqtsc})_2\text{Cl}$.

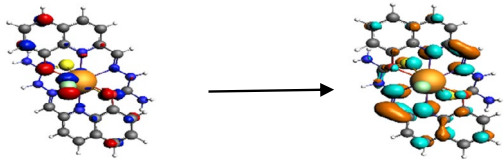
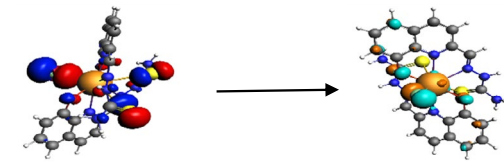
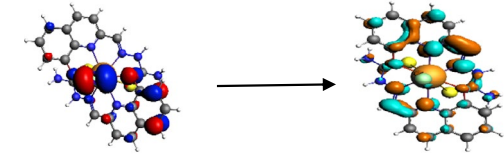
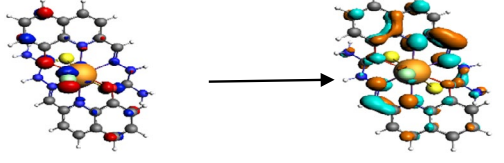
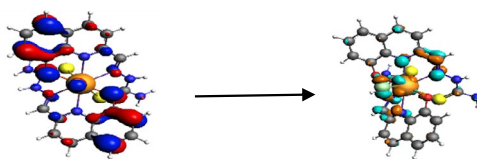
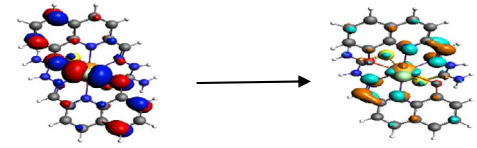
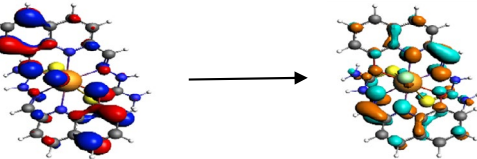
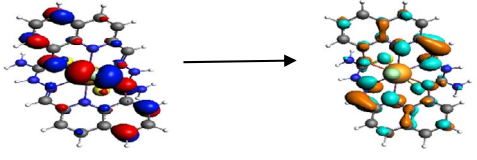
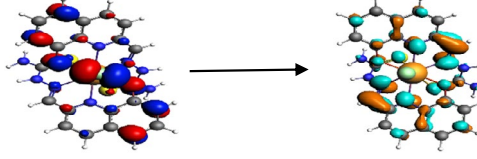
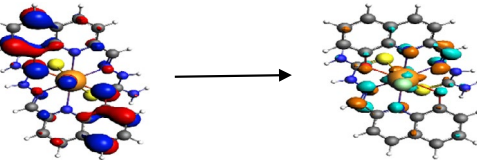
Wavelength (nm)	FMO involved in transitions	% contribution
317	 <p>HOMO (96α) 58% Eu^{3+}</p> <p>LUMO+4 (99α) 55% hqtsc</p>	63.8
341	 <p>HOMO-19 (84α) 40% Cl and 30% hqtsc</p> <p>LUMO (97α) 50% Eu^{3+}</p>	56.6
384	 <p>HOMO-1 (95α) 46% Cl and 30% hqtsc</p> <p>LUMO+2 (98α) 60% hqtsc</p>	67.9
410	 <p>HOMO (96α) 58% Eu^{3+}</p> <p>LUMO+2 (98α) 60% hqtsc</p>	90.1

Table 5 Most probable transitions involved in the absorption spectra of Tb(hqtsc)₂Cl

Wavelength (nm)	FMO involved in transitions	% contribution
317 nm	 <p>HOMO-4 (105aβ) 57 % hqtsc</p> <p>LUMO+3 (110aβ) 57% Tb³⁺</p>	61.9
365 nm	 <p>HOMO-1 (106aβ) 45% hqtsc and 23% Cl</p> <p>LUMO+6 (112aβ) 42% Tb³⁺ and 20% hqtsc</p>	59.1
398 nm	 <p>HOMO-3 (112aα) 60% hqtsc</p> <p>LUMO+2 (114 aα) 50% hqtsc</p>	33.6
444 nm	 <p>HOMO-2 (113aα) 28% Cl and 42% hqtsc</p> <p>LUMO+4 (115 aα) 55% hqtsc</p>	27.6
	 <p>HOMO-2 (113aα) 28% Cl and 42% hqtsc</p> <p>LUMO+4 (115 aα) 55% hqtsc</p>	32.6
	 <p>HOMO-4 (105aβ) 57% hqtsc</p> <p>LUMO+1 (109aβ) 53% Tb³⁺</p>	30.2

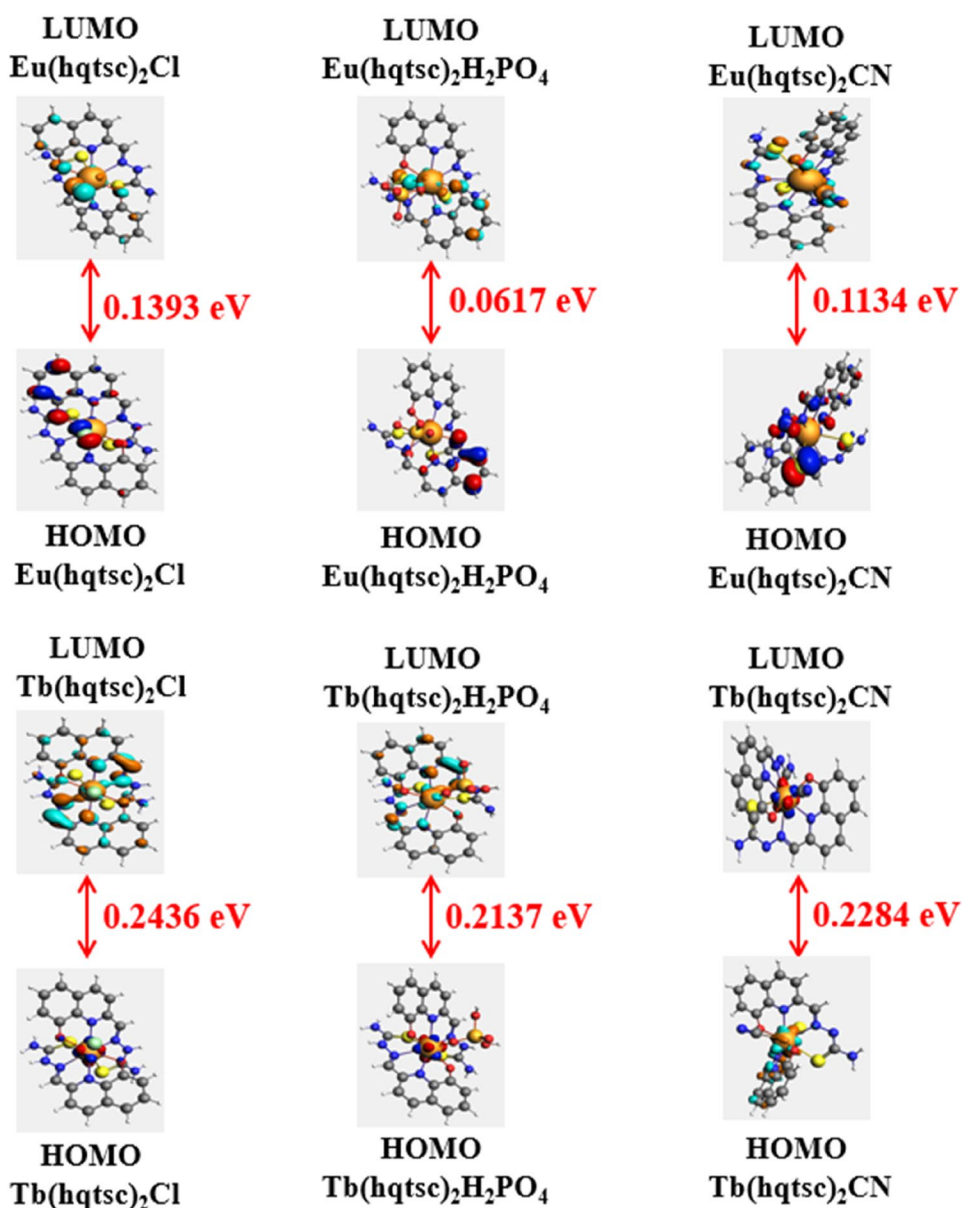
Tb(hqtsc)₂-H₂PO₄ is - 374.94 eV and for Tb(hqtsc)₂-CN is - 366.61 eV. The results show that the total binding energy of 2 and 3 decreases in the presence of H₂PO₄⁻ and CN⁻ ions, and they become more stable. Also, from Fig. 14, it is seen that the HOMO to LUMO energy gap of both complexes decreases when they form complexes with H₂PO₄⁻ and CN⁻ ions. Both the complexes are expected to be more stable with H₂PO₄⁻ and CN⁻ than Cl⁻ anion and hence replace chloride. The new complexes obtained have different spectral properties; therefore, 2 and 3 can sense H₂PO₄⁻ and CN⁻ ions.

Experimental

Materials and measurements

All of the reagents and compounds listed were obtained from TCI and Sigma Aldrich and were utilised without additional purification. All the solvents (DMSO, DMF, diethyl ether, acetone, methanol, ethanol) were from CDH and Loba Chemie, which were dried through standard methods before use. The FT-IR spectra were obtained using KBr pellets and an IR Affinity-1S Shimadzu spectrophotometer in the frequency range of 4000–400 cm⁻¹. Electrospray mass spectral analyses (ESI-MS) were done on XEVO G2-XS QTOF mass spectrophotometer. ¹H and ¹³C NMR spectra for the

Fig. 14 HOMO–LUMO energy gap of the Eu³⁺ and Tb³⁺ anion complexes



ligand and complexes were collected in deuterated DMSO on Bruker Advance Neo 500 MHz spectrometer. UV–Visible studies were performed on Horiba scientific Duetta spectrophotometer using quartz cell having path length 1 cm. The fluorescence spectra were measured in DMF on an Agilent Technologies Cary Eclipse fluorescence spectrophotometer with slit width 10. All the potentiometric titrations were done on Orion star A111 pH meter from Thermo Scientific using Thermo-Fischer Ross electrode (8102BNUWP) in highly aqueous medium i.e Water: DMSO in 9:1 v/v ratio. Theoretical calculations were done using AMS suite [60]. The elemental analysis for the sulphur [61] and chlorine were estimated quantitatively by the gravimetric method, and Eu and Tb were done by complexometric titration using EDTA [62].

Synthesis

Synthesis of hqtsc

8-Hydroxyquinoline-2-carbaldehyde (0.519 g, 3 mmol) dissolved in 15 ml of ethanol was mixed with the solution of thiosemicarbazide (0.273 g, 3 mmol) prepared in 15 ml hot ethanol and the resultant solution was refluxed for 5 h with constant stirring [54]. The resulting pale-yellow residue (0.628 g, 85.16%) was washed several times with ethanol and diethyl ether and dried in a vacuum. Molecular Formula: $C_{11}H_{10}N_4OS$; M.P: 248 °C; IR (KBr, cm^{-1}): 3689 (OH), 3387, 3248 (NH_2), 3153 (NH), 1539 (C=N), 1327 (C=S), 939 (C–S); 1H NMR (500 MHz, DMSO- d_6 , δ ppm): 11.86 (s, 1H, –NH–), 9.82 (s, 1H, –OH), 8.44 (d, 1H, Ar–H), 8.42 (s, 1H, – NH_2), 8.32 (s, 1H, –CH=N), 8.29 (d, 1H, Ar–H), 8.26 (s, 1H, – NH_2), 7.44 (t, 1H, Ar–H), 7.38 (d, 1H, Ar–H), 7.11 (d, 1H, Ar–H). ^{13}C (500 MHz, DMSO- d_6 , δ ppm): 178.39 (s, C=S), 153.31 (s, C–OH) 142.31 (s, C=N), 151.74, 138.05, 136.05, 128.69, 127.99, 118.35, 117.66, 112.00 (C of aromatic rings). HRMS (ES) $^+$: m/z [M + H] $^+$: 247.0653 (found : 247.0664).

Synthesis of [Eu(hqtsc) $_2$ Cl]

0.2 g (0.81 mmol) of ligand hqtsc was suspended in 10 ml methanol, followed by a few drops of 1M NaOH to maintain pH 8.0. The resulting mixture was changed into an orange-colored solution. A solution of $EuCl_3 \cdot 6H_2O$ (0.149 g, 0.40 mmol) in 5 ml ethanol was slowly added under a nitrogen atmosphere while the precipitate started forming. After complete addition, the suspension was stirred at room temperature for 2 h. The dark red compound was then filtered, washed multiple times with methanol and diethyl ether, and dried under a vacuum. Yield: 82%; Solubility: DMSO and DMF; Molar conductance: $13.5 \text{ ohm}^{-1} \text{ cm}^2 \text{ mol}^{-1}$; HRMS (positive ions) m/z [ML_2]: exact mass: 643.0190; found:

643.0215 calculated for $C_{22}H_{18}N_8O_2S_2Eu^{3+}$; elemental analyses (%) Exp. (Calc.): Eu 22.41 (22.41), S 9.44 (9.46), Cl 5.22 (5.23); IR (νcm^{-1}): 1535 (C=N), 1273 (C=S), 495 (Eu–N); 439; (Eu–O).

Synthesis of [Tb(hqtsc) $_2$ Cl]

The terbium polyhedral was synthesized using a method similar to that used for the europium compound. $TbCl_3 \cdot 6H_2O$ (0.151 g, 0.40 mmol) in 5 ml ethanol was stirred for 2 h with the alkaline solution of ligand. The resulting cherry red precipitate was filtered, washed 4–5 times with methanol and diethyl ether, and dried in vacuum. Yield: 84%; Solubility: DMSO and DMF; Molar conductance: $14.8 \text{ ohm}^{-1} \text{ cm}^2 \text{ mol}^{-1}$; HRMS (positive ions) m/z [ML_2]: exact mass: 649.0231; found: 649.0266 calculated for $C_{22}H_{18}N_8O_2S_2Tb^{3+}$; Elemental analyses (%) Exp. (Calc.): Tb 23.21 (23.20), S 9.33 (9.36), Cl 5.10 (5.18); IR cm^{-1}): 1535 (C=N), 1271 (C=S), 497 (Tb–N); 441 (Tb–O).

TGA studies

TGA of samples were obtained on Perkin Elmer STA 6000 thermal analyser by using a platinum crucible. Thermogravimetric studies were performed under a nitrogen atmosphere, rate of heating and temperature range was set as $20.0 \text{ }^\circ\text{C min}^{-1}$ and 40–750 °C respectively.

Potentiometric titrations

Potentiometric titrations of hqtsc and its Eu^{3+} and Tb^{3+} complexes were performed at $25 \pm 1 \text{ }^\circ\text{C}$ in a double-wall jacketed titration flask using an Orion star A111 pH meter. The glass electrode was calibrated with pH values of 4 and 9.2 buffer solutions. Potassium hydroxide (0.1 M) was standardized against 0.1 M standard KHP solution, and 0.1 M HCl solution was then standardized against the standard KOH to get accurate concentration values. The 1:2 mixture of ligand and Ln salts (Eu^{3+} , Tb^{3+}) having conc. 1×10^{-3} were acidified using 0.1 M HCl, and ionic strength was maintained with 1.0 M KCl solution. The solutions were then titrated with standardized alkali solution in pH range of 2–11. The data were fitted by a global fitting program Hyperquad [63] to calculate log β values. Species distribution curves were generated using Hyss 2009 [64].

Spectrophotometric titrations

Spectrophotometric titrations of hqtsc and its lanthanide complexes were carried out similarly to potentiometric titrations. Here, the concentration for both ligand and Ln salts was 0.5×10^{-3} in 1:2 ratio. Absorption spectra were taken in Thermo Scientific Evolution 201 UV–Vis spectrophotometer

after each addition of KOH. 2 ml solution was taken in quartz cuvette for taking the absorption spectra, and the solution was put back carefully in the titration flask for further addition of KOH. The formation constants of metal complexes were evaluated by fitting data into the computer program Hyspec [65].

Anion sensing studies

Stock solutions of $\text{Eu}(\text{hqtsc})_2\text{Cl}$ (**1**), $\text{Tb}(\text{hqtsc})_2\text{Cl}$ (**2**) and anions (tetra-*n*-butyl ammonium salts) of 1×10^{-3} M were prepared in DMF. Initially, a 3 ml solution of each complex (20×10^{-6} M) was prepared by adding 0.06 ml from the respective stock solutions of metal complexes and diluting the remaining volume with DMF. Each complex's absorbance spectra were then recorded. The interaction of both the probes with the anions was studied colorimetrically. The absorbance spectra of complexes **2** and **3** were taken by combining one equivalent of complex **2** or **3** with three equivalents of each anion separately, a 3ml cuvette solution containing 20×10^{-6} M solution of **2** or **3** and 60×10^{-6} M anion solution in DMF. The absorption spectra of the complexes in the presence of different anions were recorded. The association constant (K_a) values of the complexes with H_2PO_4^- and CN^- ions in DMF were calculated based on a B–H plot using the standard equation $K_a = 1/\text{slope}$ [66]. The slope was obtained via linear fitting the plot $1/\text{analyte concentration}$ vs. $1/\text{change in absorbance}$. The LOD calculations were computed using equation $3\sigma/\text{slope}$, where the standard deviation of the maximum absorbance of the blank (probes **2** and **3**, respectively) is represented as σ [67]. In this case, the slope is calculated by linearly fitting a plot of absorbance vs. concentration of analyte.

Computational studies

The Linux operating system was used to do the DFT computations. The probable molecular structures of compounds were built using complex build [68, 69] and initially optimized in Avogadro using the universal force field (UFF) [70, 71]. The lanthanide complexes were optimized again using the sparkle model [72, 73]. The optimized compounds were finally optimized in DFT using the AMS 2021 program. GGA-BLYP-D3-DZ/GGA-BP-86-DZ were used as an XC functionals for optimization and frequency calculations [74–76]. Model SAOP and GGA-PBE were used for the spectral calculations of the ligand and complexes, respectively.

Conclusions

Two lanthanide coordination polyhedra $\text{Eu}(\text{hqtsc})_2\text{Cl}$ and $\text{Tb}(\text{hqtsc})_2\text{Cl}$ were synthesized by employing tetradentate 8-hydroxyquinoline-based thiosemicarbazones. The

polyhedra were found to detect H_2PO_4^- and CN^- ions in DMF. They showed a naked eye color change from orange or yellow to colorless, along with the corresponding changes in the absorption spectra. It is assumed that H_2PO_4^- a hard donor replaces chloride from the respective complexes and forms a 1:1 complex– H_2PO_4^- adduct. Additionally, the europium and terbium polyhedra showed a visible color change from orange/yellow to red in the presence of CN^- ions due to the displacement of chloride ions by cyanide ions. The cyanide ions are expected to abstract a proton from each secondary –NH group of the thiosemicarbazide moiety, forming di-negative complex–CN adducts. Further, solution thermodynamic studies revealed the formation of ML_2H_2 , ML_2H_1 , ML_2 , ML_2H_{-1} , and ML_2H_{-2} complexes with high $\log \beta$. The structure of the ligand hqtsc obtained from the DFT studies matches the crystal structure of a similar molecule. The optimized Eu^{3+} and Tb^{3+} complexes were found to be non-coordinated with distorted tricapped trigonal prism geometry, demonstrating a fashionable ‘Butterfly’ appearance. The sensing mechanisms for the anions, H_2PO_4^- and CN^- are also supported through DFT studies. The novel 8HQ-based lanthanoid probes can be explored further to find suitability for applications like sensor technology and medicine to address anions overload-caused diseases.

Supplementary Information The online version contains supplementary material available at <https://doi.org/10.1007/s10847-024-01230-8>.

Author contributions Neha Kumari: Experimental work, drafting; Minati Baral: Concept, supervision, and manuscript correction; Dinesh Kumar: supervision; B K Kanungo: validation and correction.

Data availability No datasets were generated or analysed during the current study.

Declarations

Competing interests The authors declare no competing interests.

References

- Long, J., Guari, Y., Ferreira, R.A.S., Carlos, L.D., Larionova, J.: Recent advances in luminescent lanthanide based Single-Molecule Magnets. *Coord. Chem. Rev.* **363**, 57–70 (2018). <https://doi.org/10.1016/j.ccr.2018.02.019>
- Yin, F., Liu, Z., Yang, J., Zhou, L.-P., Tian, C.-B., Sun, Q.-F.: Self-assembly of triple-stranded lanthanide molecular quasi-lantern containing 2,2'-bipyridine receptor: luminescence sensing and magnetic property. *ACS Omega*. **8**, 24477–24484 (2023). <https://doi.org/10.1021/acsomega.3c02419>
- Lacerda, S., Tóth, É.: Lanthanide complexes in molecular magnetic resonance imaging and theranostics. *ChemMedChem*. **12**, 883–894 (2017). <https://doi.org/10.1002/cmdc.201700210>
- Jia, J.-H., Li, Q.-W., Chen, Y.-C., Liu, J.-L., Tong, M.-L.: Luminescent single-molecule magnets based on lanthanides: design strategies, recent advances and magneto-luminescent studies.

- Coord. Chem. Rev. **378**, 365–381 (2019). <https://doi.org/10.1016/j.ccr.2017.11.012>
5. Sun, L.-N., Zhang, H.-J., Meng, Q.-G., Liu, F.-Y., Fu, L.-S., Peng, C.-Y., Yu, J.-B., Zheng, G.-L., Wang, S.-B.: Near-infrared luminescent hybrid materials doped with lanthanide (Ln) complexes (Ln = Nd, Yb) and their possible laser application. *J. Phys. Chem. B.* **109**, 6174–6182 (2005). <https://doi.org/10.1021/jp044591h>
 6. Rohini, Baral, M., Kanungo, B.K.: Structural effect on the central cavity of a pendent 12N3 macrocycle on bonding and photophysical properties of Eu^{3+} and Tb^{3+} complexes: experimental and theoretical study. *J. Mol. Struct.* **1184**, 324–338 (2019). <https://doi.org/10.1016/j.molstruc.2019.02.032>
 7. Bünzli, J.-C.G., Piguet, C.: Taking advantage of luminescent lanthanide ions. *Chem. Soc. Rev.* **34**, 1048 (2005). <https://doi.org/10.1039/b406082m>
 8. Carlos, L.D., Ferreira, R.A.S., Bermudez, V.D.Z., Ribeiro, S.J.L.: Lanthanide-containing light-emitting organic–inorganic hybrids: a bet on the future. *Adv Mater.* **21**, 509–534 (2009). <https://doi.org/10.1002/adma.200801635>
 9. Vigato, P.A., Peruzzo, V., Tamburini, S.: The evolution of β -diketone or β -diketophenol ligands and related complexes. *Coord. Chem. Rev.* **253**, 1099–1201 (2009). <https://doi.org/10.1016/j.ccr.2008.07.013>
 10. Lacoste, R.G., Christoffers, G.V., Martell, A.E.: New multidentate ligands. II. Amino acids containing α -pyridyl groups. *J. Am. Chem. Soc.* **87**, 2385–2388 (1965). <https://doi.org/10.1021/ja01089a015>
 11. Vinusha, H.M., Kollur, S.P., Revanasiddappa, H.D., Ramu, R., Shirahatti, P.S., Nagendra Prasad, M.N., Chandrashekar, S., Begum, M.: Preparation, spectral characterization and biological applications of Schiff base ligand and its transition metal complexes. *Results Chem.* **1**, 100012 (2019). <https://doi.org/10.1016/j.rechem.2019.100012>
 12. Abad-Galán, L., Cieslik, P., Comba, P., Gast, M., Maury, O., Neupert, L., Roux, A., Wadehoff, H.: Excited state properties of lanthanide(III) complexes with a nonadentate bispidine ligand. *Chemistry* **27**, 10303–10312 (2021). <https://doi.org/10.1002/chem.202005459>
 13. Song, Y., Xu, H., Chen, W., Zhan, P., Liu, X.: 8-Hydroxyquinoline: a privileged structure with a broad-ranging pharmacological potential. *Med. Chem. Commun.* **6**, 61–74 (2015). <https://doi.org/10.1039/C4MD00284A>
 14. Côte-Real, L., Pósa, V., Martins, M., Colucas, R., May, N.V., Fontrodona, X., Romero, I., Mendes, F., Pinto Reis, C., Gaspar, M.M., Pessoa, J.C., Enyedy, É.A., Correia, I.: Cu(II) and Zn(II) complexes of new 8-hydroxyquinoline Schiff bases: investigating their structure, solution speciation, and anticancer potential. *Inorg. Chem.* **62**, 11466–11486 (2023). <https://doi.org/10.1021/acs.inorgchem.3c01066>
 15. Prachayasittikul, V., Prachayasittikul, V., Prachayasittikul, S., Ruchirawat, S.: 8-Hydroxyquinolines: a review of their metal chelating properties and medicinal applications. *DDDT* (2013). <https://doi.org/10.2147/DDDT.S49763>
 16. Yang, Y., Zhou, Z., Wei, Z.-Z., Qin, Q.-P., Yang, L., Liang, H.: High anticancer activity and apoptosis- and autophagy-inducing properties of novel lanthanide(III) complexes bearing 8-hydroxyquinoline-*N*-oxide and 1,10-phenanthroline. *Dalton Trans.* **50**, 5828–5834 (2021). <https://doi.org/10.1039/D1DT00450F>
 17. Qin, Q.-P., Wang, Z.-F., Tan, M.-X., Huang, X.-L., Zou, H.-H., Zou, B.-Q., Shi, B.-B., Zhang, S.-H.: Complexes of lanthanides (III) with mixed 2,2'-bipyridyl and 5,7-dibromo-8-quinolinone chelating ligands as a new class of promising anticancer agents. *Metallomics.* **11**, 1005–1015 (2019). <https://doi.org/10.1039/c9mt00037b>
 18. Xu, H.-B., Li, J., Shi, L.-X., Chen, Z.-N.: Sensitized luminescence in dinuclear lanthanide(III) complexes of bridging 8-hydroxyquinoline derivatives with different electronic properties. *Dalton Trans.* **40**, 5549 (2011). <https://doi.org/10.1039/c0dt01663b>
 19. Li, Q., Zhang, J., Cai, Y., Qu, W., Gao, G., Lin, Q., Yao, H., Zhang, Y., Wei, T.: A facile colorimetric and fluorescent cyanide chemosensor: utilization of the nucleophilic addition induced by resonance-assisted hydrogen bond. *Tetrahedron.* **71**, 857–862 (2015). <https://doi.org/10.1016/j.tet.2014.12.047>
 20. Misra, R., Jadhav, T., Dhokale, B., Mobin, S.M.: Colorimetric and fluorimetric detection of fluoride and cyanide ions using tri and tetra coordinated boron containing chromophores. *Dalton Trans.* **44**, 16052–16060 (2015). <https://doi.org/10.1039/C5DT02356D>
 21. Liu, X.-M., Li, Y.-P., Zhang, Y.-H., Zhao, Q., Song, W.-C., Xu, J., Bu, X.-H.: Ratiometric fluorescence detection of fluoride ion by indole-based receptor. *Talanta.* **131**, 597–602 (2015). <https://doi.org/10.1016/j.talanta.2014.08.017>
 22. Miyaji, H., Sato, W., Sessler, J.L.: Naked-eye detection of anions in dichloromethane: colorimetric anion sensors based on Calix[4]pyrrole. *Angew. Chem. Int. Ed.* **39**, 1777–1780 (2000). [https://doi.org/10.1002/\(SICI\)1521-3773\(20000515\)39:10%3c1777::AID-ANIE1777%3e3.0.CO;2-E](https://doi.org/10.1002/(SICI)1521-3773(20000515)39:10%3c1777::AID-ANIE1777%3e3.0.CO;2-E)
 23. Miyaji, H., Sato, W., Sessler, J.L., Lynch, V.M.: A 'building block' approach to functionalized calix[4]pyrroles. *Tetrahedron Lett.* **41**, 1369–1373 (2000). [https://doi.org/10.1016/S0040-4039\(99\)02295-9](https://doi.org/10.1016/S0040-4039(99)02295-9)
 24. Ghosh, T., Maiya, B.G., Samanta, A.: A colorimetric chemosensor for both fluoride and transition metal ions based on dipyrrolyl derivative. *Dalton Trans.* (2006). <https://doi.org/10.1039/b510469f>
 25. Sessler, J.L., Andrioletti, B., Anzenbacher, P., Black, C., Eller, L., Furuta, H., Jursíková, K., Maeda, H., Marquez, M., Mizuno, T., Try, A.: 2,3-Dipyrrolylquinoxaline-based anion sensors. In: Moyer, B.A., Singh, R.P. (eds.) *Fundamentals and Applications of Anion Separations*, pp. 71–85. Springer, Boston (2004)
 26. Kim, T., Swager, T.M.: A fluorescent self-amplifying wavelength-responsive sensory polymer for fluoride ions. *Angew. Chem. Int. Ed.* **42**, 4803–4806 (2003). <https://doi.org/10.1002/anie.200352075>
 27. Hassell-Hart, S., Speranzini, E., Srikanth, S., Hossack, E., Roe, S.M., Fearon, D., Akinbosede, D., Hare, S., Spencer, J.: Synthesis of a thiazole library via an iridium-catalyzed sulfur ylide insertion reaction. *Org. Lett.* **24**, 7924–7927 (2022). <https://doi.org/10.1021/acs.orglett.2c02996>
 28. James, T.D., Sandanayake, K.R.A.S., Shinkai, S.: Novel photoinduced electron-transfer sensor for saccharides based on the interaction of boronic acid and amine. *J. Chem. Soc. Chem. Commun.* (1994). <https://doi.org/10.1039/c39940000477>
 29. Yamamoto, H., Momiyama, N.: Rich chemistry of nitroso compounds. *Chem. Commun.* (2005). <https://doi.org/10.1039/b503212c>
 30. Otón, F., Tárraga, A., Molina, P.: A bis-guanidine-based multi-signaling sensor molecule that displays redox-ratiometric behavior or fluorescence enhancement in the presence of anions and cations. *Org. Lett.* **8**, 2107–2110 (2006). <https://doi.org/10.1021/ol060495i>
 31. Lowe, A.J., Long, B.M., Pfeffer, F.M.: Conformationally preorganised hosts for anions using norbornane and fused [n]polynorbornane frameworks. *Chem. Commun.* **49**, 3376 (2013). <https://doi.org/10.1039/c3cc40702k>
 32. Rosenthal, A.K., Ryan, L.M.: Nonpharmacologic and pharmacologic management of CPP crystal arthritis and BCP Arthropathy and periarticular syndromes. *Rheum. Dis. Clin. N. Am.* **40**, 343–356 (2014). <https://doi.org/10.1016/j.rdc.2014.01.010>
 33. Yung, B.Y., Kornberg, A.: Membrane attachment activates dnaA protein, the initiation protein of chromosome replication

- in *Escherichia coli*. Proc. Natl Acad. Sci. U.S.A. **85**, 7202–7205 (1988). <https://doi.org/10.1073/pnas.85.19.7202>
34. Shen, X., Mizuguchi, G., Hamiche, A., Wu, C.: A chromatin remodelling complex involved in transcription and DNA processing. *Nature*. **406**, 541–544 (2000). <https://doi.org/10.1038/35020123>
35. Chowdhury, B., Khatua, S., Dutta, R., Chakraborty, S., Ghosh, P.: Bis-heteroleptic ruthenium(II) complex of a triazole ligand as a selective probe for phosphates. *Inorg. Chem.* **53**, 8061–8070 (2014). <https://doi.org/10.1021/ic5010598>
36. Lohar, S., Pal, S., Mukherjee, M., Maji, A., Demitri, N., Chattopadhyay, P.: A turn-on green channel Zn²⁺ sensor and the resulting zinc(II) complex as a red channel HPO₄²⁻ ion sensor: a new approach. *RSC Adv.* **7**, 25528–25534 (2017). <https://doi.org/10.1039/C7RA02175E>
37. Sen, S., Mukherjee, M., Chakrabarty, K., Hauli, I., Mukhopadhyay, S.K., Chattopadhyay, P.: Cell permeable fluorescent receptor for detection of H₂PO₄⁻ in aqueous solvent. *Org. Biomol. Chem.* **11**, 1537 (2013). <https://doi.org/10.1039/c2ob27201f>
38. Albaaj, F., Hutchison, A.J.: Hyperphosphataemia in renal failure: causes, consequences and current management. *Drugs*. **63**, 577–596 (2003). <https://doi.org/10.2165/00003495-200363060-00005>
39. Young, E.W., Albert, J.M., Satayatham, S., Goodkin, D.A., Pisoni, R.L., Akiba, T., Akizawa, T., Kurokawa, K., Bommer, J., Piersa, L., Port, F.K.: Predictors and consequences of altered mineral metabolism: the Dialysis Outcomes And Practice Patterns Study. *Kidney Int.* **67**, 1179–1187 (2005). <https://doi.org/10.1111/j.1523-1755.2005.00185.x>
40. Badugu, R.: A wavelength-ratiometric pH sensitive probe based on the boronic acid moiety and suppressed sugar response. *Dyes Pigments*. **61**, 227–234 (2004). <https://doi.org/10.1016/j.dyepig.2003.10.011>
41. DiCesare, N., Lakowicz, J.R.: New sensitive and selective fluorescent probes for fluoride using boronic acids. *Anal. Biochem.* **301**, 111–116 (2002). <https://doi.org/10.1006/abio.2001.5476>
42. Badugu, R., Lakowicz, J.R., Geddes, C.D.: Cyanide-sensitive fluorescent probes. *Dyes Pigments*. **64**, 49–55 (2005). <https://doi.org/10.1016/j.dyepig.2004.04.002>
43. Takano, R.: The treatment of leprosy with cyanocuprol. *J. Exp. Med.* **24**, 207–211 (1916). <https://doi.org/10.1084/jem.24.2.207>
44. Erdemir, S., Malkondu, S.: On-site and low-cost detection of cyanide by simple colorimetric and fluorogenic sensors: smartphone and test strip applications. *Talanta*. **207**, 120278 (2020). <https://doi.org/10.1016/j.talanta.2019.120278>
45. Parker, D.: Luminescent lanthanide sensors for pH, pO₂ and selected anions. *Coord. Chem. Rev.* **205**, 109–130 (2000). [https://doi.org/10.1016/S0010-8545\(00\)00241-1](https://doi.org/10.1016/S0010-8545(00)00241-1)
46. Pope, S.J.A., Burton-Pye, B.P., Berridge, R., Khan, T., Skabara, P.J., Faulkner, S.: Self-assembly of luminescent ternary complexes between seven-coordinate lanthanide(III) complexes and chromophore bearing carboxylates and phosphonates. *Dalton Trans.* (2006). <https://doi.org/10.1039/b600598e>
47. Gunnlaugsson, T., Leonard, J.P.: Responsive lanthanide luminescent cyclen complexes: from switching/sensing to supramolecular architectures. *Chem. Commun.* (2005). <https://doi.org/10.1039/b418196d>
48. Piccinelli, F., Leonzio, M., Bettinelli, M., Monari, M., Grazioli, C., Melchior, A., Tolazzi, M.: Tuning of the sensing properties of luminescent Eu³⁺ complexes towards the nitrate anion. *Dalton Trans.* **45**, 3310–3318 (2016). <https://doi.org/10.1039/C5DT04665C>
49. Leonard, J.P., Gunnlaugsson, T.: Luminescent Eu(III) and Tb(III) complexes: developing lanthanide luminescent-based devices. *J. Fluoresc.* **15**, 585–595 (2005). <https://doi.org/10.1007/s10895-005-2831-9>
50. Huang, S.-Y., Qian, M., Pierre, V.C.: A combination of factors: tuning the affinity of Europium receptors for phosphate in water. *Inorg. Chem.* **58**, 16087–16099 (2019). <https://doi.org/10.1021/acs.inorgchem.9b02650>
51. Martinon, T.L.M., Ramakrishnam Raju, M.V., Pierre, V.C.: Kinetically Inert macrocyclic Europium(III) receptors for phosphate. *Inorg. Chem.* **62**, 10064–10076 (2023). <https://doi.org/10.1021/acs.inorgchem.2c03833>
52. Wang, Y.-W., Liu, S.-B., Yang, Y.-L., Wang, P.-Z., Zhang, A.-J., Peng, Y.: A Terbium(III)-complex-based on-off fluorescent chemosensor for phosphate anions in aqueous solution and its application in molecular logic gates. *ACS Appl. Mater. Interfaces*. **7**, 4415–4422 (2015). <https://doi.org/10.1021/am5089346>
53. Yang, D.-D., Lu, L.-P., Zhu, M.-L.: A design for detecting phosphate ions in aqueous solution by luminescent Tb-coordination polymer. *Inorg. Chim. Acta* **515**, 120030 (2021). <https://doi.org/10.1016/j.ica.2020.120030>
54. Hickey, J.L., Crouch, P.J., Mey, S., Caragounis, A., White, J.M., White, A.R., Donnelly, P.S.: Copper(II) complexes of hybrid hydroxyquinoline-thiosemicarbazone ligands: GSK3β inhibition due to intracellular delivery of copper. *Dalton Trans.* **40**, 1338–1347 (2011). <https://doi.org/10.1039/C0DT01176B>
55. Rohini, Baral, M., Kanungo, B.K.: Experimental and theoretical studies on structure, bonding and luminescence properties of Eu(III) and Tb(III) complexes of a new macrocyclic based 8HQ ligand. *J. Coord. Chem.* **72**, 1497–1523 (2019). <https://doi.org/10.1080/00958972.2019.1605064>
56. Vogel, A.I., Jeffery, G.H., Bassett, J., Mendham, J., Denney, R.C.: Vogel's Textbook of Quantitative Chemical Analysis, p. 480. Longman Scientific & Technical, Harlow (1991).
57. Chaudhary, R.G., Ali, P., Gandhare, N.V., Tanna, J.A., Juneja, H.D.: Thermal decomposition kinetics of some transition metal coordination polymers of fumaroyl bis (paramethoxyphenylcarbamide) using DTG/DTA techniques. *Arab. J. Chem.* **12**, 1070–1082 (2019). <https://doi.org/10.1016/j.arabjc.2016.03.008>
58. Gomes, L.M.F., Vieira, R.P., Jones, M.R., Wang, M.C.P., Dyrager, C., Souza-Fagundes, E.M., Da Silva, J.G., Storr, T., Beraldo, H.: 8-Hydroxyquinoline Schiff-base compounds as antioxidants and modulators of copper-mediated Aβ peptide aggregation. *J. Inorg. Biochem.* **139**, 106–116 (2014). <https://doi.org/10.1016/j.jinorgbio.2014.04.011>
59. Khatua, S., Choi, S.H., Lee, J., Kim, K., Do, Y., Churchill, D.G.: Aqueous fluorometric and colorimetric sensing of phosphate ions by a fluorescent dinuclear zinc complex. *Inorg. Chem.* **48**, 2993–2999 (2009). <https://doi.org/10.1021/ic8022387>
60. Te Velde, G., Bickelhaupt, F.M., Baerends, E.J., Fonseca Guerra, C., Van Gisbergen, S.J.A., Snijders, J.G., Ziegler, T.: Chemistry with ADF. *J. Comput. Chem.* **22**, 931–967 (2001). <https://doi.org/10.1002/jcc.1056>
61. Devine, J.M., Lane, F.W.: The use of the carius method for the determination of sulfur in the less volatile petroleum oils. *J. Am. Chem. Soc.* **50**, 1707–1710 (1928). <https://doi.org/10.1021/ja01393a029>
62. Lyle, S.J., Rahman, Md.M.: Complexometric titration of yttrium and the lanthanons—IA comparison of direct methods. *Talanta*. **10**, 1177–1182 (1963). [https://doi.org/10.1016/0039-9140\(63\)80170-8](https://doi.org/10.1016/0039-9140(63)80170-8)
63. Gans, P., Sabatini, A., Vacca, A.: Investigatio of equilibria in solution. Determination of equilibrium constants with the HYPERQUAD suite of programs. *Talanta* **43**, 1739–1753 (1996). [https://doi.org/10.1016/0039-9140\(96\)01958-3](https://doi.org/10.1016/0039-9140(96)01958-3)
64. Alderighi, L., Gans, P., Ienco, A., Peters, D., Sabatini, A., Vacca, A.: Hyperquad simulation and speciation (HySS): a utility program for the investigation of equilibria involving soluble and partially soluble species. *Coord. Chem. Rev.* **184**, 311–318 (1999). [https://doi.org/10.1016/S0010-8545\(98\)00260-4](https://doi.org/10.1016/S0010-8545(98)00260-4)

65. Segoviano-Garfias, J.J.N., Zanor, G.A., Ávila-Ramos, F., Bivián-Castro, E.Y., Rubio-Jiménez, C.A.: Spectrophotometric determination of formation constants of Iron(III) complexes with several ligands. *Chemistry*, **4**, 701–716 (2022). <https://doi.org/10.3390/chemistry4030050>
66. Benesi, H.A., Hildebrand, J.H.: A spectrophotometric investigation of the interaction of iodine with aromatic hydrocarbons. *J. Am. Chem. Soc.* **71**, 2703–2707 (1949). <https://doi.org/10.1021/ja01176a030>
67. Currie, L.A.: Detection and quantification limits: origins and historical overview. Adapted from the Proceedings of the 1996 Joint Statistical Meetings (American Statistical Association, 1997). Original title: “Foundations and future of detection and quantification limits”. Contribution of the National Institute of Standards and Technology; not subject to copyright. *Anal. Chim. Acta* **391**, 127–134 (1999). [https://doi.org/10.1016/S0003-2670\(99\)00105-1](https://doi.org/10.1016/S0003-2670(99)00105-1)
68. Taylor, M.G., Burrill, D.J., Janssen, J., Batista, E.R., Perez, D., Yang, P.: Architector for high-throughput cross-periodic table 3D complex building. *Nat Commun.* **14**, 6176 (2023). <https://doi.org/10.1038/s41467-023-42034-7>
69. Munguba, G.H.L., Urquiza-Carvalho, G.A., Silva, F.T., Simas, A.M.: The complex build algorithm to set up starting structures of lanthanoid complexes with stereochemical control for molecular modeling. *Sci. Rep.* **11**, 21493 (2021). <https://doi.org/10.1038/s41598-021-99525-0>
70. Hanwell, M.D., Curtis, D.E., Lonie, D.C., Vandermeersch, T., Zurek, E., Hutchison, G.R.: Avogadro: an advanced semantic chemical editor, visualization, and analysis platform. *J. Cheminform.* **4**, 17 (2012). <https://doi.org/10.1186/1758-2946-4-17>
71. Rappe, A.K., Casewit, C.J., Colwell, K.S., Goddard, W.A., Skiff, W.M.: UFF, a full periodic table force field for molecular mechanics and molecular dynamics simulations. *J. Am. Chem. Soc.* **114**, 10024–10035 (1992). <https://doi.org/10.1021/ja00051a040>
72. Dutra, J.D.L., Filho, M.A.M., Rocha, G.B., Freire, R.O., Simas, A.M., Stewart, J.J.P.: Sparkle/PM7 lanthanide parameters for the modeling of complexes and materials. *J. Chem. Theory Comput.* **9**, 3333–3341 (2013). <https://doi.org/10.1021/ct301012h>
73. Freire, R.O., Simas, A.M.: Sparkle/PM6 parameters for all lanthanide trications from La(III) to Lu(III). *J. Chem. Theory Comput.* **6**, 2019–2023 (2010). <https://doi.org/10.1021/ct100192c>
74. Peverati, R., Truhlar, D.G.: An improved and broadly accurate local approximation to the exchange–correlation density functional: the MN12-L functional for electronic structure calculations in chemistry and physics. *Phys. Chem. Chem. Phys.* **14**, 13171 (2012). <https://doi.org/10.1039/c2cp42025b>
75. Van Lenthe, E., Baerends, E.J.: Optimized Slater-type basis sets for the elements 1–118. *J. Comput. Chem.* **24**, 1142–1156 (2003). <https://doi.org/10.1002/jcc.10255>
76. Rosa, A., Baerends, E.J., Van Gisbergen, S.J.A., Van Lenthe, E., Groeneveld, J.A., Snijders, J.G.: Electronic spectra of $M(\text{CO})_6$ ($M = \text{Cr}, \text{Mo}, \text{W}$) revisited by a relativistic TDDFT approach. *J. Am. Chem. Soc.* **121**, 10356–10365 (1999). <https://doi.org/10.1021/ja990747t>

Publisher's Note Springer Nature remains neutral with regard to jurisdictional claims in published maps and institutional affiliations.

Springer Nature or its licensor (e.g. a society or other partner) holds exclusive rights to this article under a publishing agreement with the author(s) or other rightsholder(s); author self-archiving of the accepted manuscript version of this article is solely governed by the terms of such publishing agreement and applicable law.